USE OF AIRS AND MODIS THERMAL INFRARED CHANNELS

TO RETRIEVE ICE CLOUD PROPERTIES

A Thesis

by

CHRISTOPHER ROGERS YOST

Submitted to the Office of Graduate Studies of
Texas A&M University
in partial fulfillment of the requirements for the degree of

MASTER OF SCIENCE

December 2006

Major Subject: Atmospheric Sciences

USE OF AIRS AND MODIS THERMAL INFRARED CHANNELS

TO RETRIEVE ICE CLOUD PROPERTIES

A Thesis

by

CHRISTOPHER ROGERS YOST

Submitted to the Office of Graduate Studies of
Texas A&M University
in partial fulfillment of the requirements for the degree of

MASTER OF SCIENCE

Approved by:

Chair of Committee,   Ping Yang
Committee Members, Jerry North
                                  Thomas Wilheit
                                  George Kattawar
Head of Department, Richard Orville

December 2006

Major Subject: Atmospheric Sciences

ABSTRACT

Use of AIRS and MODIS Thermal Infrared Channels to Retrieve Ice Cloud Properties.

(December 2006)

Christopher Rogers Yost, B.S., Texas A&M University

Chair of Advisory Committee: Dr. Ping Yang

In this study, we use thermal infrared channels to retrieve the optical thickness and effective particle radius of ice clouds. A physical model is used in conjunction with Atmospheric Infrared Sounder (AIRS) temperature and water vapor profiles to simulate the top-of-atmosphere (TOA) brightness temperatures (BTs) observed by the Moderate Resolution Imaging Spectroradiometer (MODIS) for channels located at 8.5, 11.0, and 12.0 μm (1176, 909, and 833 cm^{-1}). The model is initially validated by comparing simulated clear-sky BTs to MODIS-observed clear-sky BTs. We also investigate the effect of introducing a +3 K bias in the temperature profile, a +3 K bias in the surface temperature, and a +20% bias in the water vapor profile in order to test the sensitivity of the model to these inputs. For clear-sky cases, the simulated TOA BTs agree with MODIS to within 2-3 K. The model is then extended to simulate thermal infrared BTs for cloudy skies, and we infer the optical thickness and effective radius of ice clouds by matching MODIS-observed BTs to calculations. The optical thickness retrieval is reasonably consistent with the MODIS Collection 5 operational retrieval for optically thin clouds but tends to retrieve smaller particle sizes than MODIS.

DEDICATION

This thesis is dedicated to my father, Ronald Paul Yost, for his encouragement in everything from athletics to academics.

ACKNOWLEDGMENTS

Finally, I wish to thank my friends for their support and my family for instilling in me the patience and work ethic required to complete this thesis.

TABLE OF CONTENTS

LIST OF FIGURES

FIGURE   Page

LIST OF TABLES

1. INTRODUCTION

Clouds of all types have some degree of influence on the climate of Earth. They generally reflect incoming solar radiation back to space and emit longwave radiation back to the surface of the planet. Depending on their microphysical structure and spatial and temporal distributions, clouds can have either a net warming or cooling effect on the climate. The study of ice clouds (e.g., cirrus, cirrostratus) is especially complicated because ice particles tend to have complex irregular shapes, as opposed to water clouds, which are composed of spherical or nearly spherical droplets. Therefore the effect of ice clouds on Earth's climate is a major uncertainty, despite dedicated attempts to determine their radiative forcing (Ramanathan et al. 1989, McFarquhar et al. 2000). In order to model the future climate of Earth, we must be able to mathematically describe the radiative properties of different cloud types. This is presently accomplished by using parameters such as ice water content (IWC), liquid water content (LWC), effective emissivity, cloud fraction, cloud optical thickness (COT), and effective particle size (EPS) to predict the effects of clouds on the energy budget of the atmosphere (Wielicki et al. 1995). Satellite measurements are often used to derive these parameters since satellite-borne instruments provide the only way to quickly obtain global information about the atmosphere.

Several studies have demonstrated the usefulness of using visible and shortwave-infrared (SWIR) channels to retrieve cloud properties such as optical thickness and effective size. Nakajima and King (1990) showed that visible and SWIR reflectances

---

This thesis follows the style of *Journal of the Atmospheric Sciences*.

are useful for simultaneously retrieving COT and EPS. In their retrieval of COT and EPS, a radiative transfer (RT) model is used to simulate reflectances for several combinations of COT and EPS. Satellite-observed reflectances are then compared to the simulated values, and the retrieved COT and EPS is the pair that gives the best match to the observed data.

Meyer et al. (2004) used a similar approach to retrieve the optical thickness of tropical cirrus clouds. In this study, spectral bands near 0.66 and 1.38 μm were used in the retrieval. Because 1.38-μm radiation is strongly absorbed by water vapor, most of the radiation observed by satellites in this spectral band is reflected off the tops of high cirrus clouds. There is a nearly linear relationship between 0.66 and 1.38-μm reflectances, so the 0.66-μm reflectance can then be used to retrieve the visible optical thickness of high cirrus clouds. This method is also sensitive to optically thin ($\tau < 3$) cirrus clouds.

Although visible and SWIR channels have been very successful in retrieving cloud properties during the day, satellite instruments are generally not sensitive enough to detect radiation in these channels at night. It was discovered that certain sensors are sensitive enough to detect lightning at night (Kidder and Vonder Haar 1995), but normally the visible and SWIR signal from Earth is too weak for most sensors to detect in the absence of sunlight. Fortunately, many studies have demonstrated the ability to derive cloud properties from infrared (IR) radiation, which is available both day and night.

A study showing the utility of thermal infrared channels for cloud retrievals was performed by Inoue (1985). He used Advanced Very High Resolution Radiometer (AVHRR) channels 4 (10.5-11.5 μm) and 5 (11.5-12.5 μm) to derive the temperature and effective emissivity of semitransparent (i.e., optically thin) cirrus clouds. He referred to this method as the bi-spectral method. In the literature, the use of two channels in the 8-13 μm spectral region to retrieve cloud properties is also referred to as the split-window technique.

Wei et al. (2004) used IR channels on the Atmospheric Infrared Sounder (AIRS) to retrieve the optical thickness of ice clouds. Their method involved using a fast RT model to create a lookup table of brightness temperatures (BTs) for channels near 6.3, 6.4, 8.0, and 11.0 μm (1587, 1559, 1231, and 900 cm^{-1}). Again, this method was shown to be valid for optically thin ice clouds.

Huang et al. (2004) developed an algorithm to simultaneously retrieve COT and EPS for ice clouds by using high spectral resolution data in the atmospheric window region (8-13 μm). Their model calculations showed that the slope of the BT spectrum between 10.4-12.7 μm (790-960 cm^{-1}) is sensitive to EPS, while the BT spectrum between 8-9.5 μm (1050-1250 cm^{-1}) is sensitive to COT. The model performed calculations for a range of optical thicknesses and effective sizes. The BT spectrum that best matched the observed spectrum was used to simultaneously retrieve COT and EPS. Using this technique, the maximum retrievable optical thickness and effective size is approximately 8 and 80 μm respectively.

Ackerman et al. (1990), Strabala et al. (1994), Baum et al. (2000b) and Menzel et al. (2002) have demonstrated the use of thermal IR channels to determine cloud phase. They discovered that the brightness temperature difference (BTD) between an 8-μm band and an 11-μm band ($BT_8 - BT_{11}$) is negative for clear skies but positive for ice clouds due to the increased 11-μm absorption in the presence of ice. BTDs between the 11- and 12-μm bands ($BT_{11} - BT_{12}$) are positive when viewing a cirrus cloud or clear skies. The inclusion of the 8-μm band thus removes the ambiguity of using the 11- and 12-μm bands alone. Since the absorption coefficient of ice increases more from 8-11 μm than from 11-12 μm, $BT_8 - BT_{11}$ is generally larger than $BT_{11} - BT_{12}$ when viewing ice clouds, but the exact threshold for the difference between the two pairs of channels is dependent on the amount of water vapor in the atmosphere and the proximity of the 8- and 11-μm bands to water vapor absorption lines (Strabala et al. 1994). This forms the basis for the trispectral technique used to determine cloud phase using three channels in the thermal IR window.

Even though algorithms using visible and SWIR channels to retrieve cloud properties have proven to be highly effective, they are limited in use to daytime only, at least for now. However, IR window channels clearly can provide a wealth of information at night, when visible and SWIR methods are rendered inoperable. The goal of this thesis is to continue our understanding of IR remote sensing, which will ultimately enhance our knowledge of cloud radiative forcing and climate change. The rest of this thesis is structured as follows. Section 2 will provide a detailed explanation of the methods used for this research as well as some background information about the

satellite instruments used to carry out the research. In Section 3, the results of a sensitivity study will be presented. Section 4 will describe in more detail the method used in this study for simultaneously retrieving COT and EPS from IR window channels, and the results will be presented and compared to other studies. Section 5 will assess the utility of this retrieval method and discuss the context for its practical use.

2. INSTRUMENTATION AND METHODOLOGY

In this study, we use thermal IR channels in the atmospheric window (8-13 μm) to retrieve the optical and microphysical properties of ice clouds. In particular, we are interested in using channels near 8.5, 11.0 and 12.0 μm to simultaneously retrieve COT and effective particle radius (EPR). These three channels are located in a strong ice absorption band, so the TOA radiances in these channels are strongly influenced by the presence of ice clouds. The TOA radiances decrease as the optical depth of ice clouds increases. Therefore we can obtain optical thickness information from the TOA BTs of these channels. Furthermore, the difference between the single-scattering albedos at 8.5 and 11 μm increases with decreasing particle size, as shown in Figure 1. Therefore, some particle size information can be obtained from the BTD between these two channels, particularly for small particles. Duda and Spinhirne (1996) also used bands at 11 and 12 μm to simultaneously obtain the optical thickness and EPS of contrails. In this study, we use both pairs of channels to simultaneously retrieve COT and EPR for ice phase clouds from pre-computed lookup tables.

The primary obstacle hindering nighttime remote sensing is the lack of a spectral channel that is relatively insensitive to optical thickness (Minnis et al. 1995). Visible channels are relatively insensitive to particle size and are independent of cloud temperature, whereas thermal IR channels are highly sensitive to both cloud temperature and optical thickness for optical depths less than approximately 6. Once this threshold is exceeded, there is no further sensitivity to optical depth, limiting cloud retrievals to cases
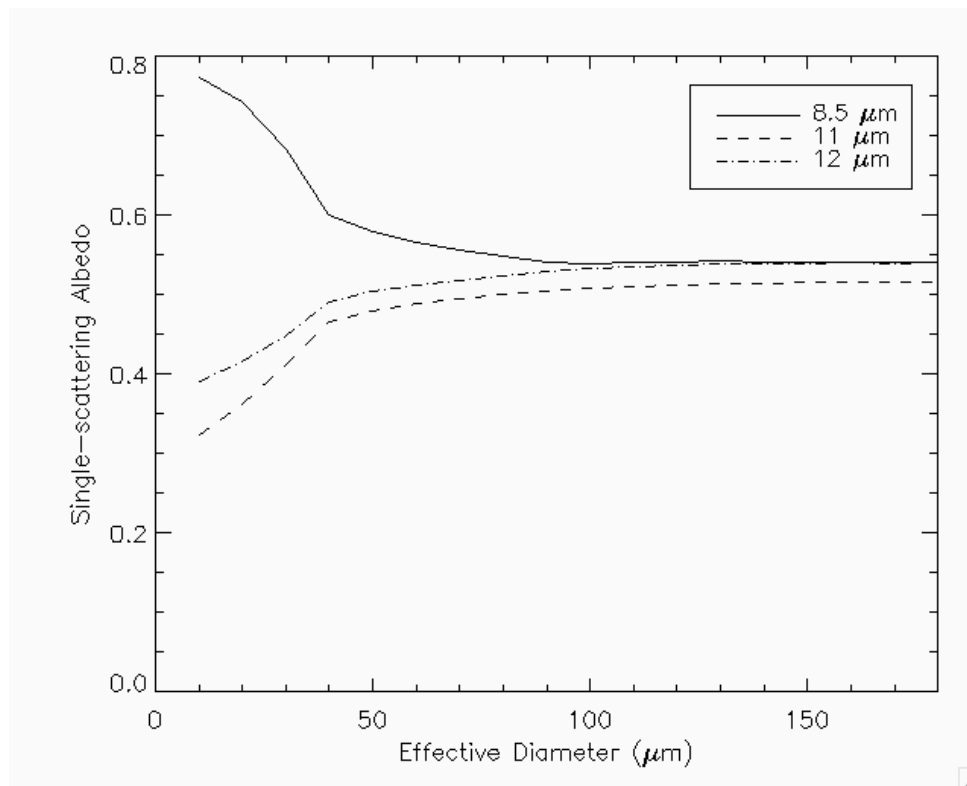
FIG. 1. Single-scattering albedo as a function of effective diameter for spectral bands located at 8.5, 11, and 12 μm.

where the optical thickness does not exceed 6. Nevertheless, IR remote sensing continues to be the only method for obtaining nighttime cloud properties. MODIS, with its relatively high spatial resolution and wide spectral coverage, promises to make IR cloud retrievals more precise than ever.

Several tools are needed to perform this retrieval. We use the discrete-ordinate RT code developed by Stamnes et al. (1988) known as DISORT to perform all the RT calculations. In addition, we use measurements from the Moderate Resolution Imaging Spectroradiometer (MODIS) and the Atmospheric Infrared Sounder (AIRS) to perform the RT calculations and the cloud retrieval. This section provides the necessary background information about AIRS, DISORT, and MODIS and explains their role in this research. Furthermore, we provide some background information on the so-called correlated k-distribution method for the calculation of gaseous absorption and the ice crystal model used in this study.

a. AIRS

On May 4, 2002, the National Aeronautics and Space Administration (NASA) launched the Aqua satellite as part of the Earth Observing System (EOS). Aqua is equipped with an array of state-of-the-art instruments designed to assess the impact of natural events and human activities on the global climate and to provide a long-term global climate record (King et al. 1995). Included in this array of instruments are the Atmospheric Infrared Sounder (AIRS), the Advanced Microwave Sounding Unit

(AMSU), and the Humidity Sounder for Brazil (HSB). Together, these instruments
provide global vertical temperature, water vapor, and ozone profiles twice daily.

AIRS observes the earth and its atmosphere with 2378 channels covering the
spectral intervals 3.74-4.61 μm (2674-2169 cm⁻¹), 6.20-8.22 μm (1613-1217 cm⁻¹) and
8.8 μm-15.4 μm (1136-649 cm⁻¹) and has a nominal spectral resolution of $\lambda/\Delta\lambda = 1200$.
Calibrated radiances, referred to as the Level 1b products, are provided to the public at
13.5-km spatial resolution. From these radiances, the Level 2 products, such as water
vapor profiles and surface temperature, are derived at 40-km horizontal spatial
resolution. The Level 1 and 2 products are available to the public in EOS Hierarchical
Data Format (EOS HDF) from the Goddard Space Flight Center (GSFC) Distributed
Active Archive Center (DAAC).

All Level 2 products are derived from the 'cloud-cleared' radiance product
(Aumann et al. 2003). Susskind et al. (2003) describes the cloud-clearing algorithm
used by AIRS/AMSU/HSB in detail. The algorithm attempts to infer what the radiances
of cloudy fields of view (FOVs) would be in the absence of any clouds. The basic idea
is to use observations from K adjacent FOVs to obtain the clear-column radiance for
channel i given by,

$$\hat{R}_i = R_{i,1} + \sum_{k=1}^{K-1} \eta_k (R_{i,1} - R_{i,K+1-k}),$$
(1)

where $\hat{R}_i$ is the clear-column radiance for channel i, $R_{i,k}$ is the channel i observation in
FOV k, and η_k are coefficients that must be solved for in order to give true values of $\hat{R}_i$

up to instrumental noise effects. The advantage of this method is that it does not require accurate modeling of the spectral emissivity, reflectivity, or transmissivity of the clouds.

The cloud-cleared radiances are used as input to derive the subsequent Level 2 data products in the following order:

1) surface skin temperature, surface spectral emissivity, and surface bidirectional reflectance of solar radiation

2) atmospheric temperature profiles

3) atmospheric moisture profiles

4) atmospheric ozone profiles

5) cloud properties.

In this study, we are primarily interested in the surface skin temperature, vertical temperature and moisture profiles, and cloud top pressure (CTP). All Level 2 products are produced at 40-km horizontal spatial resolution. Atmospheric temperature and moisture content are provided at 28 vertical pressure levels. AIRS, AMSU, and HSB (referred to simply as AIRS hereafter) together achieve a global retrieval accuracy of better than 1 K in the lower troposphere under clear and partly cloudy conditions (Aumann et al. 2003) and moisture profiles are retrieved with absolute errors less than 20% (Susskind et al. 2003). The CTP product is still under development, but an estimate of the CTP error is provided in the Level 2 products (Chahine et al. 2001).

b. Radiative transfer and DISORT

The DISORT code developed by Stamnes et al. (1988) is a numerical method for

solving the radiative transfer equation (RTE) in plane-parallel, vertically

inhomogeneous, non-isothermal, multiple scattering and emitting media. It is based

upon the well-known theory for solving the RTE described by Chandresekhar (1960).

The RTE for monochromatic radiation is given by

$$\mu \frac{dI_\lambda(\tau_\lambda, \mu, \phi)}{d\tau} = I_\lambda(\tau_\lambda, \mu, \phi) - S_\lambda(\tau_\lambda, \mu, \phi), \tag{2}$$

where $I_\lambda(\tau_\lambda, \mu, \phi)$ is the specific intensity for diffuse radiation along direction μ, ϕ at

optical depth τ_λ measured perpendicular to the surface of the medium, μ is the cosine of

the polar zenith angle, and ϕ is the azimuthal angle. S_λ represents the source function

and can be written out as

$$S_\lambda(\tau_\lambda, \mu, \phi) = \frac{\omega_\lambda(\tau_\lambda)}{4\pi} \int_0^{2\pi} \int_{-1}^1 P_\lambda(\tau_\lambda, \mu, \phi; \mu', \phi') I_\lambda(\tau_\lambda, \mu', \phi') d\mu' d\phi' + Q_\lambda(\tau_\lambda, \mu, \phi), \tag{3}$$

where $\omega_\lambda(\tau_\lambda)$ is the single-scattering albedo, and $P_\lambda(\tau_\lambda, \mu, \phi; \mu', \phi')$ is the scattering phase

function. The term Q_λ is composed of two terms, $Q_\lambda^{(thermal)}$ and $Q_\lambda^{(beam)}$, given by

$$Q_\lambda^{(thermal)}(\tau_\lambda) = [1 - \omega_\lambda(\tau_\lambda)] B_\lambda[T(\tau_\lambda)], \tag{4}$$

$$Q_\lambda^{(beam)}(\tau_\lambda, \mu, \phi) = \frac{\omega_\lambda(\tau_\lambda) I_0}{4\pi} P_\lambda(\tau_\lambda, \mu, \phi; -\mu_0, \phi_0) e^{-\tau_\lambda / \mu_0}, \tag{5}$$

respectively, where $B_\lambda(T)$ is the Planck function at wavelength λ and temperature T, and

$\mu_0 I_0$ is the incident flux. $Q_\lambda^{(thermal)}$ is the source term for thermal emission in

thermodynamic equilibrium, and $Q_\lambda^{(beam)}$ is the source term for a parallel beam incident

in direction μ_0, ϕ_0 on a non-emitting medium. The sum of $Q_\lambda^{(thermal)}$ and $Q_\lambda^{(beam)}$ gives Q_λ,

that is

$$Q_\lambda(\tau_\lambda, \mu, \phi) = Q_\lambda^{(thermal)}(\tau_\lambda) + Q_\lambda^{(beam)}(\tau_\lambda, \mu, \phi). \tag{6}$$

In RT computations involving ice particles, is it often necessary to approximate the phase function. The phase function may be expressed as a series of Legendre polynomials in order to solve Equation 2 numerically (Liou 2002). In this case, the phase function is expressed as

$$P(\cos\Theta) = \sum_{\ell=0}^{M} \tilde{\omega}_\ell P_\ell(\cos\Theta), \qquad (7)$$

where Θ is the scattering angle, and the expansion coefficient $\tilde{\omega}_\ell$ is given by

$$\tilde{\omega}_\ell = \frac{2\ell+1}{2} \int_{-1}^{1} P(\cos\Theta)P_\ell(\cos\Theta)d\cos\Theta. \qquad (8)$$

Ice particles often exhibit strong forward scattering due to diffraction, seen as a delta-function-like spike in the phase function at scattering angles near 0°. The value of the phase function at scattering angles less than about 5° can be as much as five to six orders of magnitude greater than phase function values at side scattering angles. In reality, the values of such wildly behaved phase functions are known only at a few hundred specific scattering angles. For numerical computations however, we need an approximate function that provides values at all scattering angles. A delta-function-like peak makes this a difficult task, but there are methods to solve this problem. The usual method involves truncating the phase function at a small scattering angle and removing the troublesome diffraction peak (Potter 1970). This truncation reduces the number of Legendre polynomial terms needed to represent the phase function and significantly reduces the computational burden.

The so-called δ-M method (Wiscombe 1977) is a popular method for performing phase function truncation. Using this method, the phase function is approximated as

$$P_{\delta-M}(\Theta) = \sum_{\ell=0}^{2M-1} \frac{(\tilde{\omega}_\ell - f)}{(1-f)} P_\ell(\cos\Theta), \qquad (9)$$

where M is the order of approximation, P_ℓ is a Legendre polynomial, and $\tilde{\omega}_\ell$ are phase function expansion coefficients. This method is highly accurate, requiring $M = 8$ (16 streams) for 4-6 digit accuracy for fluxes. For computing radiances however, this method is not quite sufficient. In this study, we are interested in radiance calculations, so we use a slightly different method for approximating the phase function. Hu et al. (2000) developed a method to calculate Legendre expansion coefficients c_k that minimize the relative difference ε between the actual phase $P(\Theta)$ function and the approximate phase function $P'(\Theta)$. The least-squares fitting problem

$$\frac{\partial \varepsilon}{\partial c_k} = 0, \qquad k = 0\ldots N \qquad (10)$$

is solved, where

$$\varepsilon = \sum_i w_i \left(\frac{P'(\Theta_i)}{P(\Theta_i)} - 1 \right)^2, \qquad (11)$$

and w_i is the weight for each scattering angle. This method, called the δ-fit method, produces a very good approximation of the phase function, especially at large scattering angles. This makes it an ideal tool for satellite studies.

Once the scattered energy is removed from the forward peak of the phase function, the scattering parameters must be adjusted to reflect this change. The adjusted scattering optical depth τ_s' becomes

$$\tau_s' = (1-f)\tau_s \qquad (12)$$

where f is the fraction of energy removed from the forward peak of the phase function

and τ_s is the scattering optical depth before truncation. Since the absorption optical

depth τ_a is unaffected by the truncation, the total adjusted optical depth is then given by

$$\tau' = (1 - f)\tau_s + \tau_a \tag{13}$$

The adjusted single-scattering albedo and asymmetry factor become

$$\tilde{\omega}' = \frac{(1 - f)\tilde{\omega}}{1 - f\tilde{\omega}} \tag{14}$$

and

$$g' = \frac{g - f}{1 - f}, \tag{15}$$

respectively. This adjustment of the scattering parameters is referred to in the literature

as the similarity principle (Liou 2002).

In addition to the strong forward scattering caused by diffraction, still more

forward scattering results from transmission through parallel planes of polyhedral ice

crystals at a scattering angle of 0°, called δ-transmission (Takano and Liou 1989). For

visible wavelengths, it is necessary to truncate the phase function again for δ-

transmission. Because absorption by ice increases for longer wavelengths, such as those

in the IR window, δ-transmission becomes a negligible contributor to strong forward

peaks in the phase function. It is emphasized here that no δ-transmission truncation was

necessary in this study since absorption by ice dominates the RT processes in the

thermal IR spectral region.

c. Correlated k-distribution

Any simulation of thermal IR radiances at the TOA must account for the molecular absorption of radiation in the atmosphere. In the IR window region, molecular absorption is particularly important for optically thin cirrus clouds but is less important for optically thick clouds, because emission and multiple scattering by ice particles dominate the radiative processes (Liou 1974). Contributions from molecular absorption above high cirrus clouds are generally unimportant as well. Surface and molecular emission from below the cloud penetrates optically thin cirrus clouds however, and therefore this emission must be included in the RT calculations.

Table 1 shows the principal absorbing atmospheric gases for three MODIS bands in the thermal IR spectral region. Carbon dioxide and water vapor are the infamous greenhouse gases, but other trace gases such as methane and ozone contribute a non-negligible amount of absorption. The absorption coefficient for a specific molecule at wavenumber v can be expressed as

$$k_v(p,T) = \sum_{j=1}^{N} S_j(T) f_{v,j}(p,T), \qquad j = 1, 2, ..., N \qquad (16)$$

where p is pressure, T is temperature, S_j is line intensity for the jth absorption line, and $f_{\lambda,j}$ is the normalized line shape. Databases exist that contain the line position, line intensity, and air-broadened half-width for a particular wavenumber. Traditionally, line-by-line models are used to resolve individual absorption lines using the information in these databases. This process can be rather time-consuming however, due to the extreme precision that is needed to resolve individual absorption lines. Fortunately, a more

TABLE 1. Spectral range and principal absorbing atmospheric gases for three MODIS

bands in the thermal IR window.

MODIS band	Spectral range (μm)	Principal absorbing gases
29	8.400 – 8.700	H_2O, O_3, CH_4, N_2O
31	10.780 – 11.280	H_2O, CO_2
32	11.770 – 12.270	H_2O, CO_2

efficient method, called the correlated k-distribution (CKD) method, exists to calculate molecular absorption in nonhomogeneous atmospheres.

For a homogeneous atmosphere, the transmittance within a spectral interval is dependent only on the fraction of the interval that is associated with a specific value of k (Fu and Liou, 1992). In other words, ordering the k-values within a spectral interval by wavenumber is unimportant; they can be arranged in any configuration without affecting the transmittance. Therefore, a probability distribution function (PDF) $h(k)$ can be defined where $h(k)dk$ is the fraction of Δv within which the absorption coefficient is between k and $k + \Delta k$. In the literature, this PDF is also called the k-distribution function, from which the CKD method derives its name. The spectral-mean transmittance can then be expressed as

$$T_{\bar{v}}(u) = \int_{\Delta v} e^{-k(v)u} \frac{dv}{\Delta v} = \int_0^\infty e^{-ku} h(k)dk, \tag{17}$$

where u is the pathlength. We now define a cumulative probability distribution function (CDF) $g(k)$ such that

$$g(k) = \int_0^k h(k)dk, \tag{18}$$

where $g(0) = 0$, $g(k \to \infty) = 1$, and $dg(k) = h(k)dk$. Now the spectral-mean transmittance may be expressed in terms of g as

$$T_{\bar{v}}(u) = \int_{\Delta v} e^{-k(v)u} \frac{dv}{\Delta v} = \int_0^1 e^{-k(g)u} dg, \tag{19}$$

where $k(g)$ is the inverse of $g(k)$ and called the equivalent k function. By definition, $g(k)$ is a smooth monotonically increasing function so $k(g)$ is also. This function can be integrated with ease over the g domain with only a few quadrature points, while an

integration over the wavenumber domain would be tedious and time consuming. This concept is better illustrated in Figure 2. Figure 2a shows H_2O absorption lines for a spectral band centered at 1.38 μm. The absorption coefficient as a function of wavenumber over this spectral interval is characterized by sharp peaks that are difficult to resolve without taking a very small Δk. On the other hand, integration of the CDF in Figure 2b is much easier because it is smooth and monotonically increasing in the g domain. This is the conceptual basis for the correlated k-distribution method.

The vertically nonhomogeneous nature of the atmosphere is accounted for by assuming a correlation of k-distributions at different temperatures and pressures such that the spectral transmittance can be expressed as

$$T_{\bar{v}}(u) \cong \int_0^1 \exp\left[-\sum_i k_i(g)\Delta u_i\right]dg. \tag{20}$$

As demonstrated by Liou (2002), the CKD method is exact for single lines, periodic lines, and the strong- and weak-line limits. Kratz (1995) developed correlated k-distribution routines to account for the molecular absorption in the spectral ranges of the five AVHRR channels as well as several MODIS channels. In this study, we use the correlated k-distribution method to account for molecular absorption for the MODIS channels in the thermal IR window.

d. MODIS

Also aboard the Aqua satellite is the Moderate Resolution Imaging Spectroradiometer (MODIS). It observes Earth with thirty-six carefully selected spectral

(a)

(b)
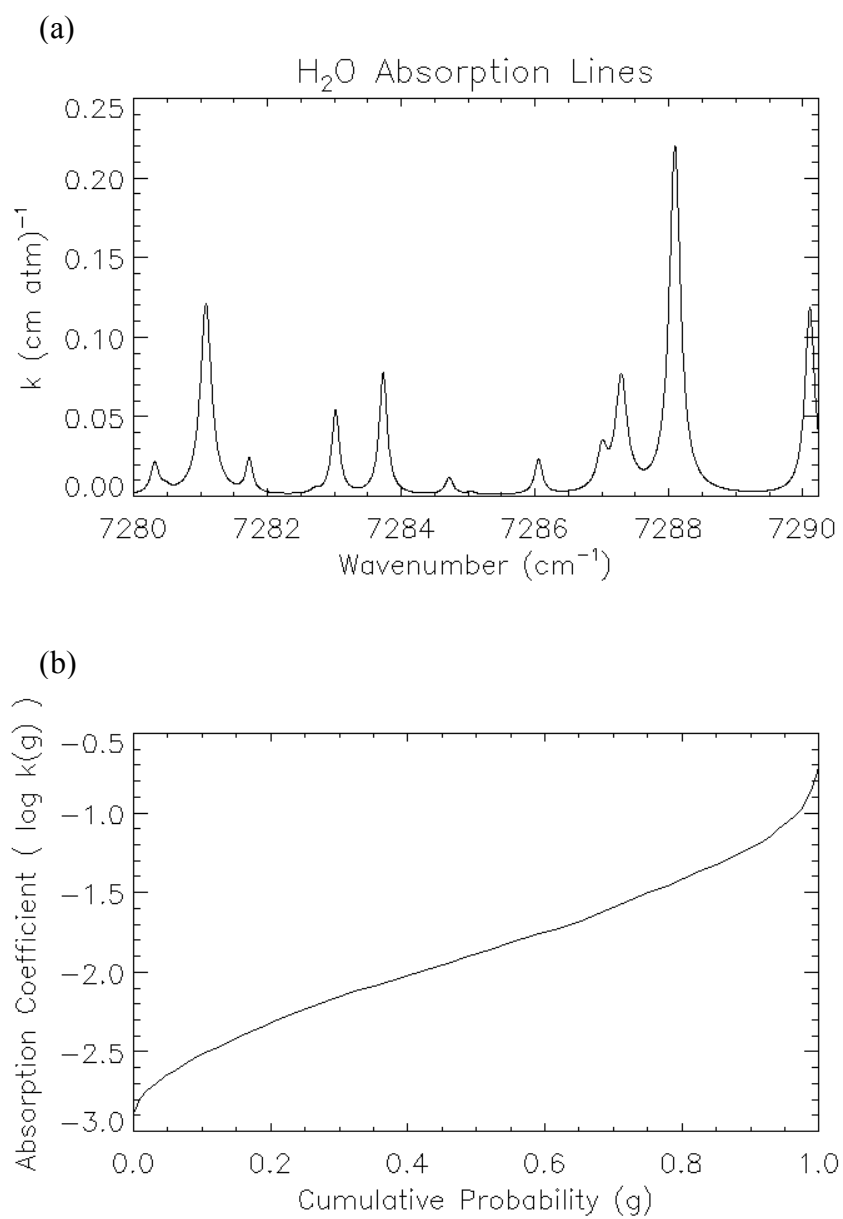
FIG. 2. Plots of (a) the absorption coefficient *k* as a function of wavenumber and (b) log

k as a function of cumulative probability *g* [line parameters are taken from Liou (2002)].

bands between 0.415 and 14.235 μm. Each spectral band was chosen for a specific purpose (e.g., thin cirrus detection or water vapor detection) in order to promote multidisciplinary studies of land-ocean-atmosphere interactions. Twenty-nine of the bands, including the IR bands, have 1-km spatial resolution. The retrieved quantities (e.g., cloud optical thickness, effective radius, and cloud top temperature), referred to as the Level 2 products, have either 1-km or 5-km spatial resolution (Platnick et al. 2003, King et al. 2003, King et al. 1997).

Like AIRS, MODIS provides calibrated radiances in their Level 1b product but at a much finer spatial resolution of 1 by 1 km at nadir. These radiances are then used as input into algorithms designed by the MODIS Science Team to retrieve cloud properties and other atmospheric quantities. The process of retrieving cloud optical and microphysical properties begins with a cloud mask (Ackerman et al. 1998). The goal of the cloud mask is to determine which FOVs are clear and which are obscured by clouds or aerosols. As many as 14 of the 36 spectral bands are used to make a final classification for each pixel, but the result is more than a simple 'clear' or 'cloudy' designation. Each pixel is determined to be either 'confidently clear', 'probably clear', 'undecided', or 'cloudy or obstructed'. Note that poor confidence in a clear scene does not necessarily mean the FOV is obstructed by clouds. Smoke, aerosols, or other contaminates could be the reason for the obstruction. The MODIS cloud mask is clear sky conservative, meaning that if even just one of the tests is highly confident that the FOV is cloudy then it is labeled as such (Ackerman et al. 1998). The cloud mask will suffer from too many cloudy reports rather than too many clear-sky reports, but in return

we can be confident that an FOV determined to be clear by the cloud mask is indeed cloud-free.

The next step in the MODIS cloud retrieval process is cloud phase determination. The MODIS cloud phase algorithm performs several threshold and reflectance ratio tests to determine if a pixel is obscured by a water or ice cloud. It is assumed that the cloud fills the entire pixel (i.e., the scene is overcast) and that it is a single-layer homogenous cloud. Currently, the algorithm makes no attempt to identify mixed-phase clouds, but an unknown cloud phase is labeled as such.

Since different look-up libraries are used to retrieve COT and EPR for water and ice clouds, the retrieval process begins once the cloud phase is determined. MODIS uses the approach of Nakajima and King (1990) mentioned in the previous section to retrieve COT and EPR. This method relies on the use of a water-absorbing band and a nonabsorbing band. The nonabsorbing band primarily provides optical thickness information while the absorbing band provides particle size information. Forward RT calculations are performed for several optical thicknesses and effective radii, producing a look-up table. The table is searched for the COT and EPR pair that gives the best match to the observed radiance. The pair of channels involved in the COT and EPR retrieval is chosen to minimize the underlying surface reflectance. The 0.65-, 0.86-, and 1.2-μm bands are nonabsorbing bands and are used over land, ocean, and ice/snow surfaces respectively (Platnick et al. 2003). The 2.1-μm band is the primary absorbing band used in the retrieval. Particle sizes retrieved from the 1.6- and 3.7-μm bands are reported as differences relative to the 2.1-μm band.

As stated before, the goal of this research is to develop an algorithm to retrieve the COT and EPR of ice clouds. Although MODIS currently retrieves COT and EPR, the algorithm is limited to daytime use only, because it uses a visible and a shortwave infrared band. In this study, we explore the possibility of using the thermal IR channels on MODIS to retrieve cloud properties, which would be useful for nighttime retrievals.

e. Ice scattering model

In recent years, an incredible amount of effort has focused on determining the single scattering properties of ice crystals. Ice crystals are much more difficult to model than water droplets, because ice crystals come in a variety of complex shapes, each with their own single-scattering properties. Intense theoretical work (Yang et al. 1997, Yang et al. 2003, Yang et al. 2005) and field campaigns (Baum et al. 2000a) have led to the development of an extensive database containing the single-scattering properties for a mixture of ice shapes that approximates those found in nature. The most recent database, described by Yang et al. (2005), Baum et al. (2005), and Nasiri et al. (2002), incorporates data gathered from the First International Satellite Cloud Climatology Project Regional Experiment (FIRE)-I, FIRE-II, Atmospheric Radiation Measurement (ARM) Program intensive observation period, Tropical Rainfall Measuring Mission (TRMM) Kwajalein Experiment (KWAJEX), and the Cirrus Regional Study of Tropical Anvils and Cirrus Layers (CRYSTAL) Florida Area Cirrus Experiment (FACE). The single-scattering properties of 1117 particle size distributions (PSDs) were analyzed and band-averaged models were developed for use by MODIS. The ice crystal structures

assumed in this model include droxtals, bullet rosettes, solid columns, plates, hollow

columns, and aggregates. The habit (or shape) percentages are a function of the

maximum dimension D of the ice particles as shown in Table 2. Yang et al. (1997)

reported that equivalent ice spheres are a poor representation of natural ice cloud

particles, but the configuration shown in Table 2 yields single-scattering properties that

better approximate the scattering features observed in natural cirrus clouds.

In these models, the particle size distribution is described by the effective

diameter D_e which is defined as

$$D_e = \frac{3}{2} \frac{\sum_{D=D_{min}}^{D_{max}} \left[\sum_{h=1}^{H} V(h,D) f(h,D) n(D) \Delta D \right]}{\sum_{D=D_{min}}^{D_{max}} \left[\sum_{h=1}^{H} A(h,D) f(h,D) n(D) \Delta(D) \right]}, \tag{21}$$

after Foot (1988) and Francis et al. (1994). D_{min} and D_{max} are the minimum and

maximum crystal sizes in the distribution, respectively, H is the number of different ice

crystal shapes (habits) considered, V is the total volume for habit h and size D, A is the

total projected area, f is the habit fraction, $n(D)$ is the number concentration of crystals,

and ΔD is the width of size bin D. When the average crystal size is calculated as a ratio

of the volume V to the projected area A, as it is here, the details of the size distribution

are relatively unimportant in specifying the bulk optical properties of cirrus clouds

(Wyser and Yang 1998). This definition is also directly related to IWC because $V =$

IWC/ρ_i, where ρ_i is the density of ice.

In section 4 we compare the results of the IR retrieval with the COT and EPR

derived by MODIS. The ice crystal bulk scattering models just described are the same

TABLE 2. Percentages of different ice crystal shapes (habits) comprising theoretical

cirrus clouds as a function of maximum ice particle dimension D in the ice scattering

model of Baum et al. (2005).

Ice particle maximum dimension (D)	Habit types and percent composition
$D < 60$ μm	100% droxtals
60 μm $< D < 1000$ μm	15% 3D bullet rosettes 50% solid columns 35% plates
1000 μm $< D < 2500$ μm	45% hollow columns 45% solid columns 10% aggregates
2500 μm $< D < 9500$ μm	97% 3D bullet rosettes 3% aggregates

ones currently used by the MODIS Collection 5 operational retrieval algorithms. We use these same models in our RT calculations in order to be consistent with the MODIS models.

f. Ice cloud property retrieval

In order to relate the roles of all the instruments and methods described in this section, a brief outline of the cloud property retrieval follows. Section 4 provides a more complete and detailed discussion. Here we introduce the basic concept used to perform the simultaneous retrieval of COT and EPR using IR channels.

The vertical thermodynamic profiles and satellite viewing geometry from AIRS are used as input for DISORT. The atmosphere is divided into a discrete number of layers, and DISORT is implemented with 4 streams to simulate cloudy-sky TOA BTs for the 8.5-, 11.0-, and 12.0-μm MODIS channels. The CKD routines developed by Kratz (1995) are used to account for molecular absorption in the atmosphere. Ice clouds are simulated in the model by using the CTP from AIRS to determine which layer in the model the cloud should occupy, and the ice crystal model simulates the single-scattering properties. Calculations are performed for optical thicknesses ranging from 0-10 and effective diameters ranging from 10-60 μm. The BTs output by DISORT are gathered into LUTs such as the ones illustrated in Figure 3. The MODIS-observed BTs and BTDs are then used to infer COT and EPS from the pre-computed LUTs. This can be understood conceptually by plotting the MODIS-observed BTs and BTDs on the LUTs and using interpolation to obtain COT and EPR. Two retrievals of COT and EPR are

(a)

(b)

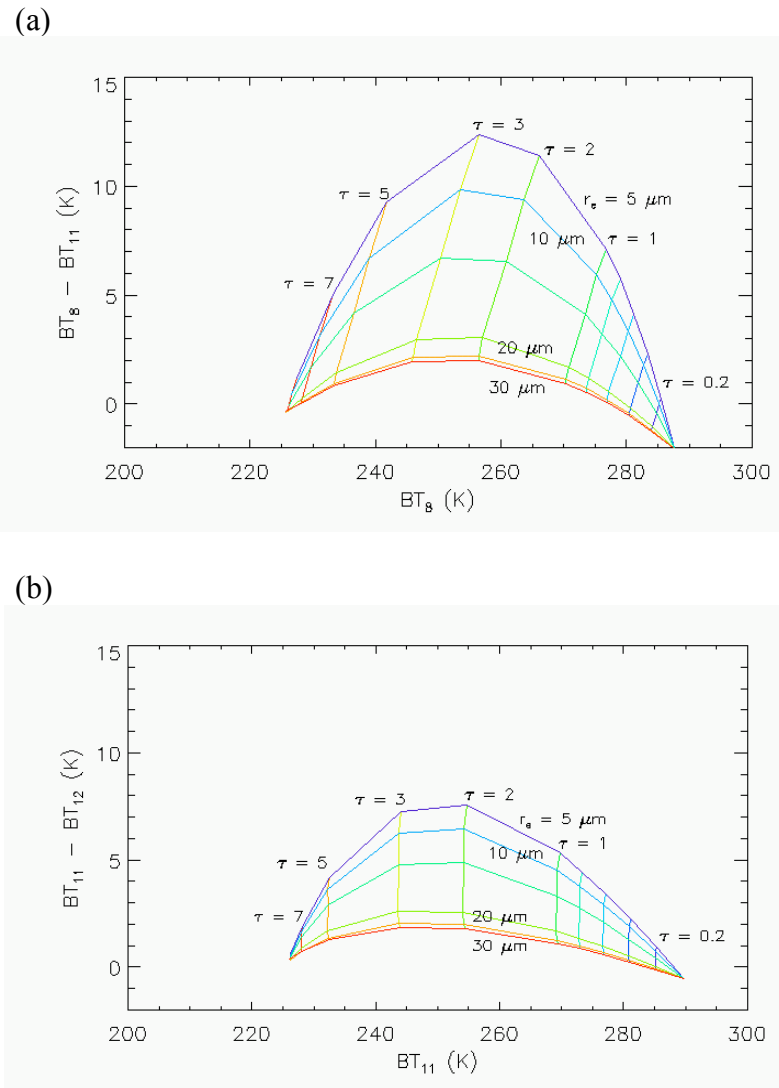FIG. 3. Sample lookup tables for (a) the 8.5/11-μm retrieval and the (b) 11/12-μm retrieval.

performed, one using the 8.5- and 11.0-μm bands and the other with the 11.0- and 12.0-μm bands. The MODIS cloud mask is used to determine which MODIS pixels within each AIRS pixel contain ice clouds. This procedure is repeated for each AIRS pixel, and the retrieval is performed for any valid MODIS pixels located within the AIRS FOV.

3. CLEAR-SKY SIMULATION AND SENSITIVITY STUDY

a. Clear-sky BT simulation

Before performing the retrieval of COT and EPR, we compare simulated clear-sky BTs to those observed by MODIS. We also investigate the sensitivity of the simulated BTs to certain parameters in the model such as the vertical temperature and moisture profiles, and surface temperature. The reasons for this are twofold. First of all, the resolution of the AIRS Level 2 products is rather coarse compared to the MODIS Level 2 products. One temperature profile, moisture profile, and surface temperature from AIRS must be used to represent a 40 km by 40 km area at nadir. For viewing angles away from nadir, the pixels span an even larger region. We want to know how variations in the thermodynamics profiles and surface temperature will affect the simulated BTs, because these parameters are certain to vary at least slightly over such a large area. Secondly, we want to know the effect of errors in the AIRS profiles due to clouds or instrument uncertainty. Under clear or partially cloudy conditions, AIRS can generally retrieve temperature profiles with RMS errors less than 1 K and moisture profiles with absolute errors less than 20% (Susskind et al. 2003). For completely cloudy scenes, the errors could be larger. Furthermore, since we are using some data that is not directly observed but is instead derived by an algorithm, any errors in the original observations and in the assumptions of the algorithm will filter through to the BT simulations. This part of the study will determine which parameters the RT calculations are most sensitive to.

First, a simulation of clear-sky BTs was performed for the 8.5-, 11.0-, and 12.0-μm MODIS bands. AIRS provides temperature and moisture profiles at 28 pressure levels, but in our model we interpolate the profiles to 35 levels. We execute the simulation only for those pixels deemed 'confidently clear' by the MODIS cloud mask in order to minimize errors caused by any cloud and aerosol contamination; 'probably clear' pixels were not included. We also limit this simulation to ocean scenes to avoid large variations in the surface emissivity. Ocean surface emissivity varies insignificantly in the 8-12 μm spectral region, so we assume a spectral surface emissivity of 0.99 for all three channels in this study. The viewing geometry for each pixel is obtained from the MODIS Level-2 products, and the simulation is run at the same resolution (1 km) as the MODIS Level-1b calibrated radiances.

We apply this simulation to a MODIS granule over the tropical Western Pacific Ocean, just east of Australia. Figure 4a shows a false color image of the granule, and Figure 4b shows an image of the MODIS cloud mask. Note in Figure 4b that 'probably cloudy' and 'probably clear' determinations are typically located at cloud edges where partial cloudiness and cloud shadows become problems.

Figures 5a, 6a, and 7a show the results of the simulated clear-sky TOA BTs, denoted BT_S, for MODIS channels 29, 31, and 32 (8.5, 11.0, and 12.0 μm), respectively. Figures 5b, 6b, and 7b show the MODIS-observed BTs (BT_O), and Figures 5c, 6c, and 7c show the difference between the MODIS-observed BTs and the simulated BTs ($BT_O - BT_S$). The simulation compares quite well to MODIS, with most differences less than about 2-3 K, but it is evident from Figures 5c, 6c, and 7c that the simulation tends to

(a)
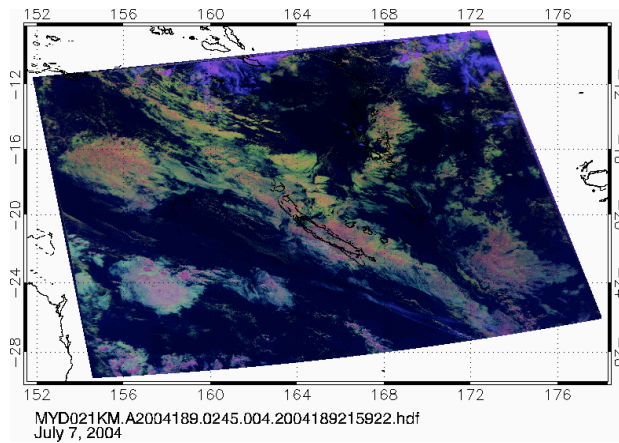
(b)
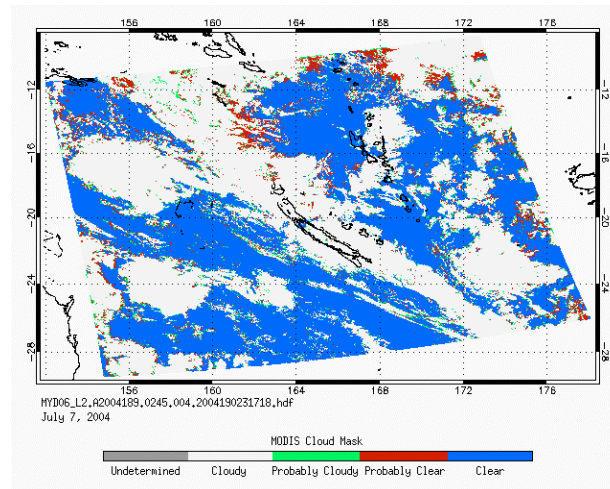
FIG. 4. Images of (a) a 0.65- (red), 2.13- (green) and 11.0-μm (blue) false-color

composite and (b) the MODIS cloud mask.
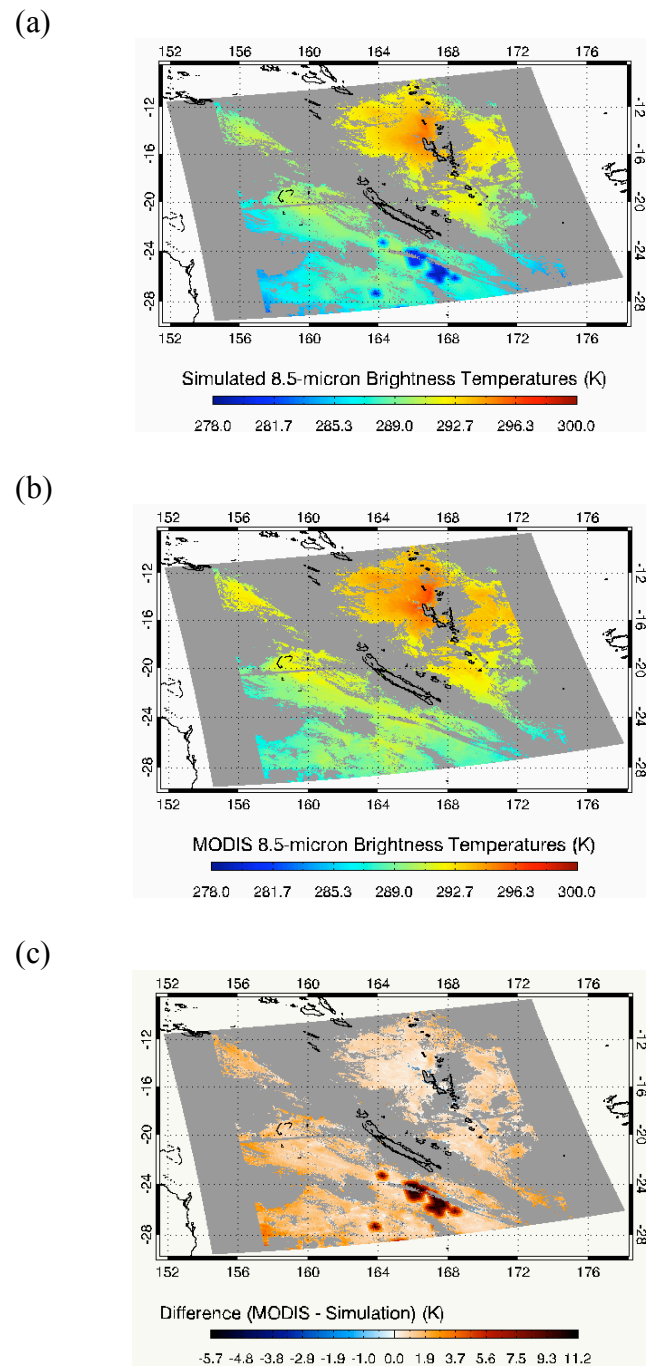
FIG. 5. Images of the clear-sky 8.5-μm (a) simulated brightness temperatures, (b) MODIS-observed brightness temperatures, and (c) the difference between the MODIS and the simulated brightness temperatures.

(a)

Simulated 11.0-micron Brightness Temperatures (K)

278.0   281.7   285.3   289.0   292.7   296.3   300.0

(b)

MODIS 11.0-micron Brightness Temperatures (K)

278.0   281.7   285.3   289.0   292.7   296.3   300.0

(c)

Difference (MODIS - Simulation) (K)

-7.0 -5.8 -4.7 -3.5 -2.3 -1.2 0.0 1.9 3.9 5.8 7.8 9.7 11.7

FIG. 6. Images of the clear-sky 11.0-μm (a) simulated brightness temperatures, (b) MODIS-observed brightness temperatures, and (c) the difference between the MODIS and the simulated brightness temperatures.

(a)

(b)

(c)
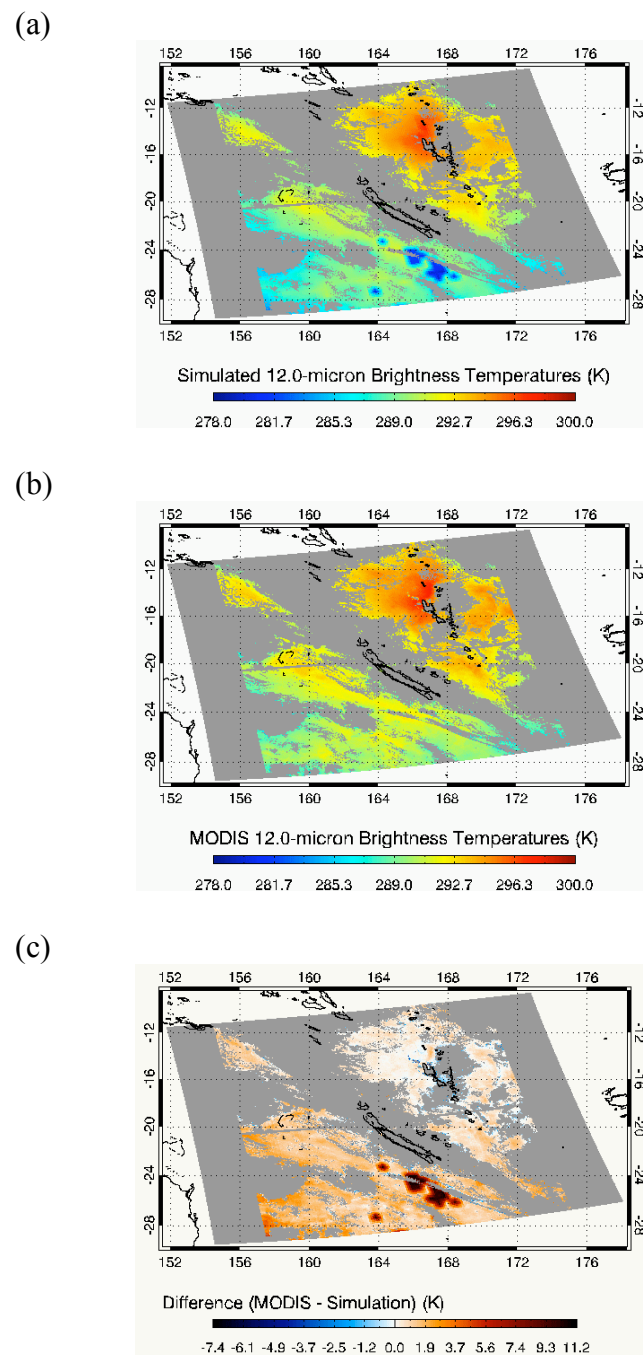
FIG. 7. Images of the clear-sky 12.0-μm (a) simulated brightness temperatures, (b) MODIS-observed brightness temperatures, and (c) the difference between the MODIS and the simulated brightness temperatures.

underestimate BTs when compared to MODIS. Note the large difference located near

25°S latitude and 166°E longitude. Here the simulation differs from the MODIS

observations by as much as 12 K. The reason for this discrepancy is evident by looking

at the image of the AIRS surface temperature product shown in Figure 8. Anomalously

low surface temperatures are found at the same location.   It seems unlikely that these

low surface temperatures are caused by cloud contamination since these pixels were

flagged 'confidently clear' by MODIS. Furthermore, the MODIS BT images show no
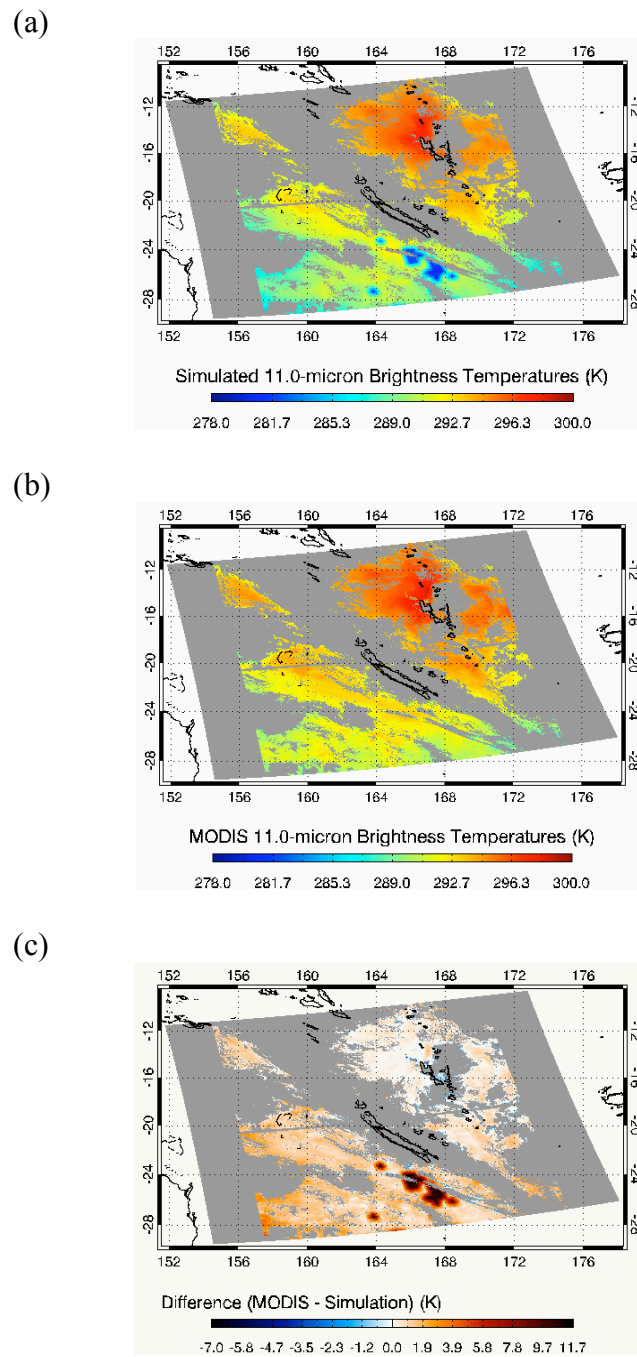
evidence of any unexpected features. While the cause of the abnormally low surface

temperatures in this region is unknown, it is clear that the low surface temperatures are

the cause for such large differences between the observed and simulated radiances.

b. Sensitivity study

     We now investigate the sensitivity of the simulation to the temperature profile,

water vapor profile, and surface temperature. We expect the simulated BTs to be more

sensitive to the surface temperature than to the air temperature, so we examine these

parameters separately. First we introduce a +3 K bias into every level of the temperature

profiles excluding the surface skin temperature. Figure 9 shows the percent relative

difference (PRD) between the previously simulated BTs and the biased BTs for a subset

of approximately 300 MODIS pixels. The error introduced by a +3 K bias in every level

of the temperature profile ranges from about 0.2-0.7%, or approximately 0.5-2.0 K. The

largest errors occur for the 12.0-μm channel, while the 11.0-μm channel appears to be
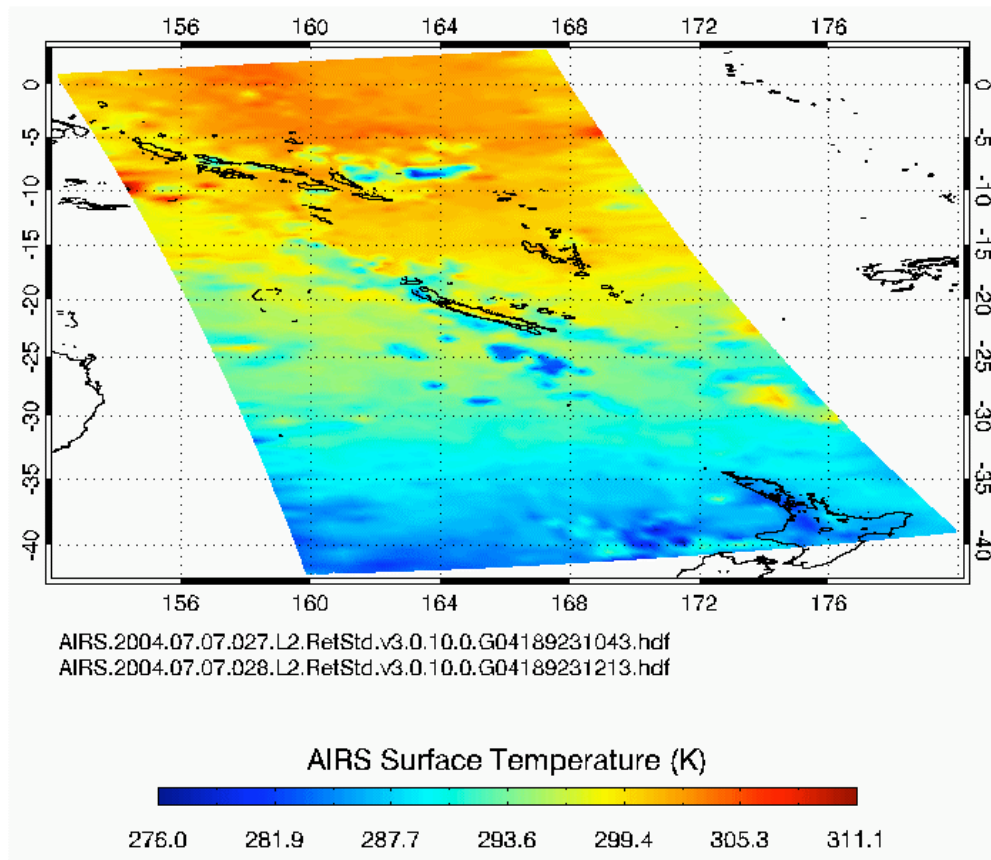
least sensitive to the air temperature.

FIG. 8. The AIRS surface temperature product corresponding to the MODIS granule shown in Figure 4.

(a)

(b)

(c)

FIG. 9. The percent relative difference between the unbiased and biased (a) 8.5-, (b) 11.0-μm, and (c) 12.0-μm brightness temperatures. A +3 K bias was introduced into every level of the temperature profile in the biased simulation.

Next we investigate the error introduced by a 20% increase in the water vapor mixing ratio at every level of the moisture profile. Figure 10 shows the results for the same pixels shown in Figure 9. In this case, the mixing ratio bias reduces the BTs by about 0.1-0.6% (0.3-2 K). The 12.0-μm channel is most sensitive, while the 8.5-μm shows the weakest sensitivity.

Now we investigate the error associated with a +3 K bias in the surface skin temperature. Figure 11 shows the results for the same subset of pixels. The PRD here between the unbiased and biased BTs is about 0.5-0.8% (1.5-2.5 K). The 11.0-μm channel is most sensitive to the surface temperature.

c. Summary

Under clear-sky conditions, the model simulates MODIS-observed BTs quite well, with most differences less than about 2-3 K. Differences much larger than this were traced back to the AIRS surface temperature product, though the original source of the error may not have originated in the AIRS surface temperature algorithm. Whatever the original cause, the same problem is not evident in the MODIS images, so the problem is probably limited to the AIRS instrument only. It seems unlikely that cloud contamination is the cause, because the MODIS cloud mask was extremely confident that the pixels were cloud-free.

A +3 K bias in the temperature profile, a +3 K bias in the surface skin temperature, and a +20% bias in the water vapor mixing ratio all caused errors on the order of 1-3 K, although the bias in the surface temperature caused errors in the high end
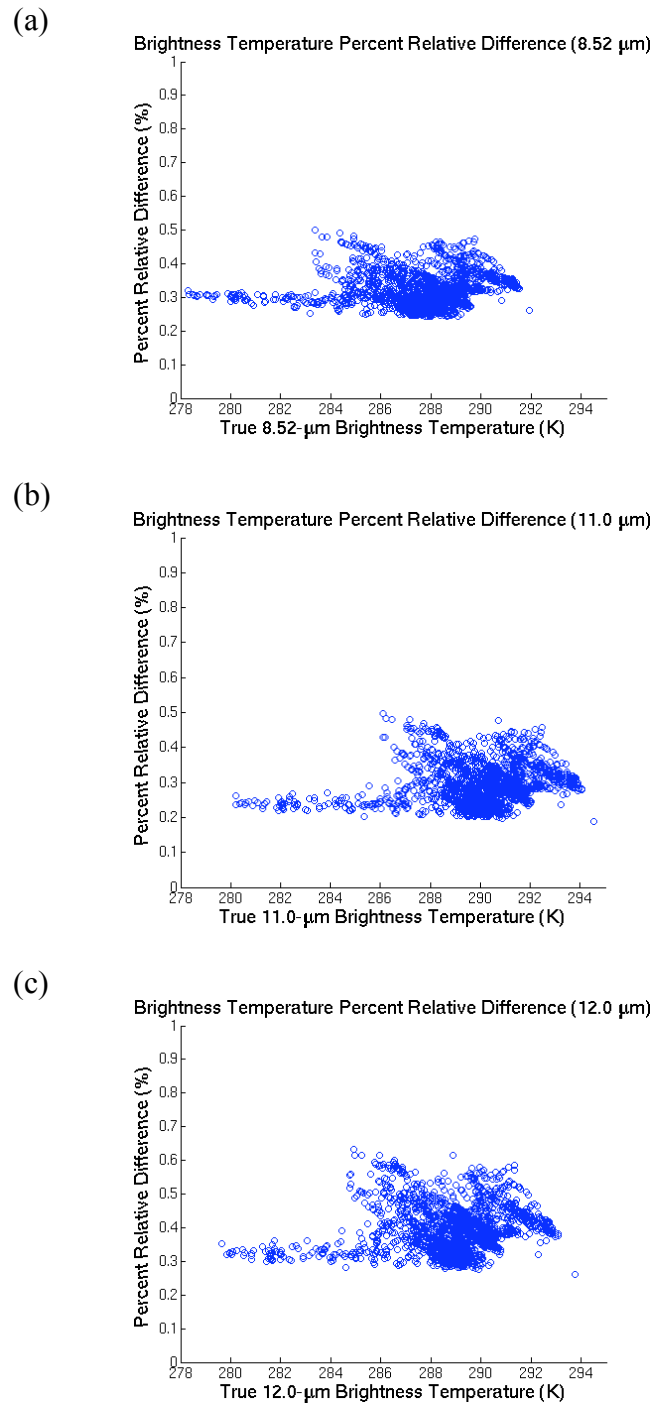
(a)

(b)

(c)
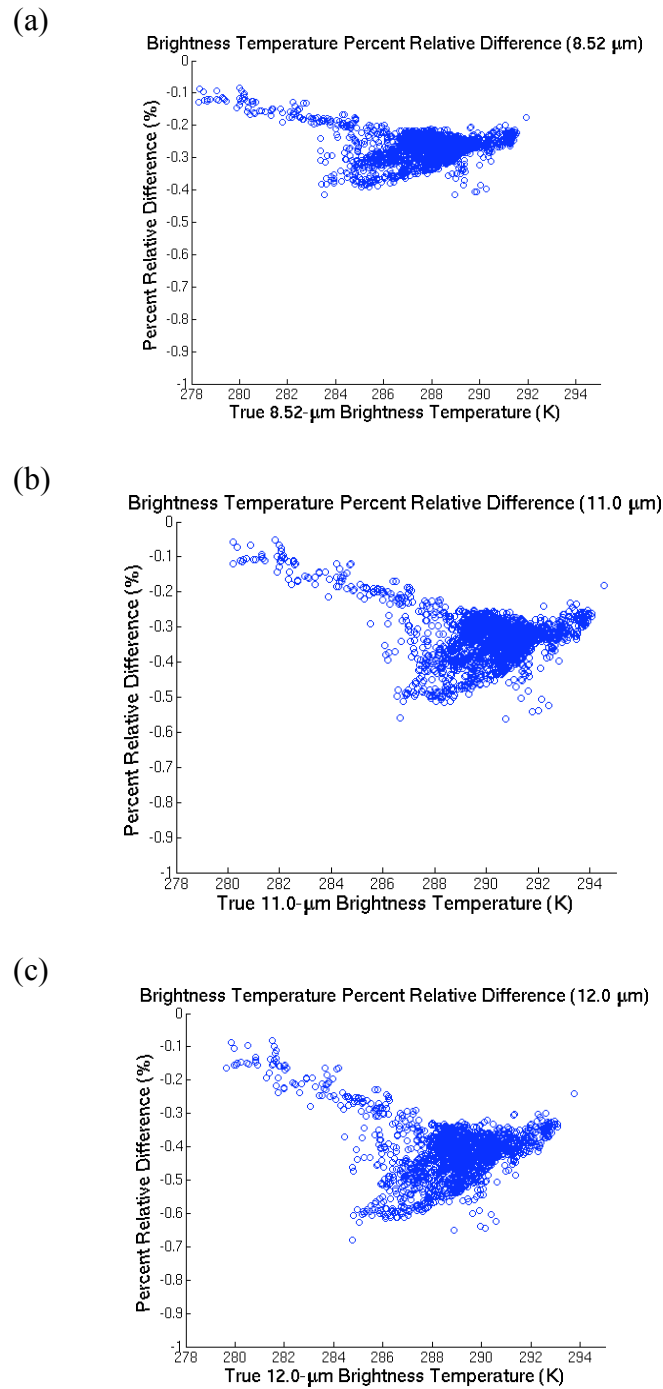
FIG. 10. The percent relative difference between the unbiased and biased (a) 8.5-, (b) 11.0-μm, and (c) 12.0-μm brightness temperatures. A +20% bias was introduced into every level of the water vapor mixing ratio profile in the biased simulation.

(a)

(b)

(c)
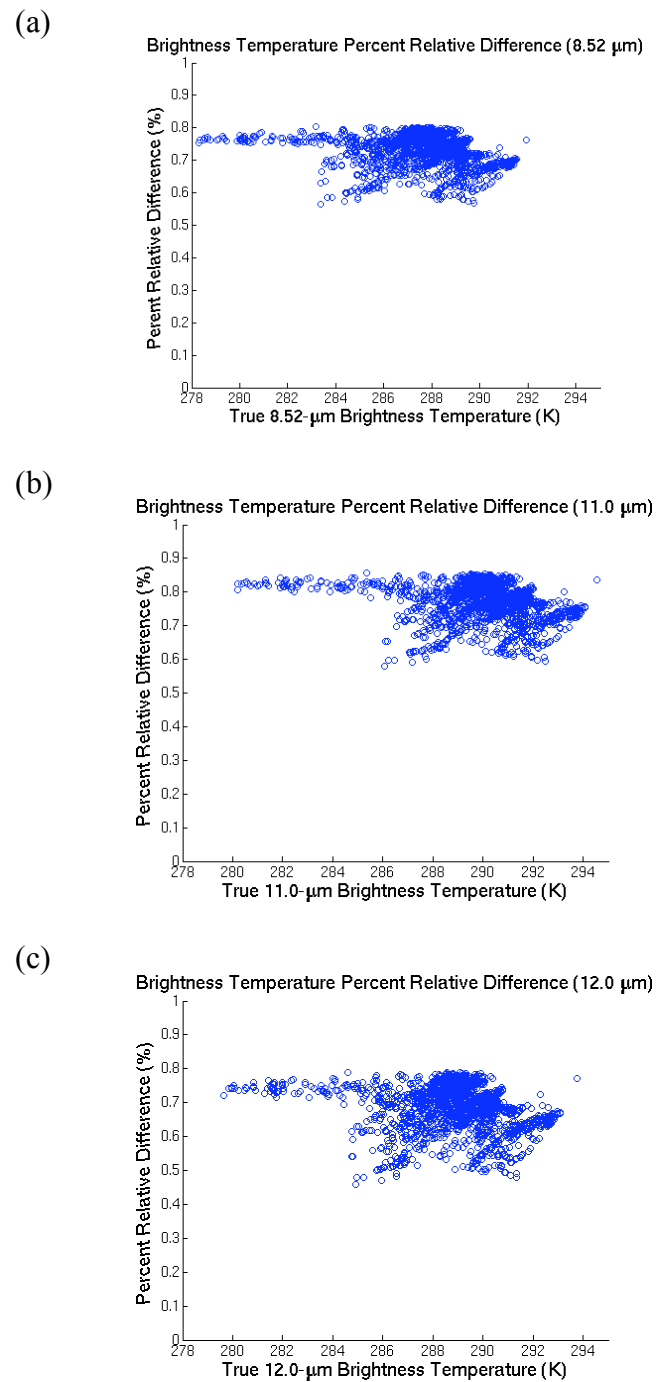
FIG. 11. The percent relative difference between the unbiased and biased (a) 8.5-, (b) 11.0-μm, and (c) 12.0-μm brightness temperatures. A +3 K bias was introduced into the surface temperature in the biased simulation.

of this range. As expected, the simulation is more sensitive to the surface temperature than the air temperature, since the weighting function for these three channels peaks at the surface. In the absence of any interpolation, one AIRS pixel must be used to simulate MODIS BTs over a region at least as large as 40 km by 40 km, so we have assumed that the temperature profile, moisture profile, and surface temperature do not vary significantly within the AIRS pixels. The results of the sensitivity study indicate that the model can simulate MODIS-observed BTs reasonably well if this is an appropriate assumption. The differences between the MODIS-observed BTs and the unbiased simulated BTs were about the same magnitude as the errors caused by reasonable biases introduced into the input parameters. As long as the profiles and surface temperature do not vary greatly and the surface is fairly homogeneous, then the model should function reasonably well over an ocean surface under clear-sky conditions.

4. CLOUD PROPERTY RETRIEVAL RESULTS

a. Results

We now apply the simulation to cloudy scenes and use MODIS-observed BTs to infer the COT and EPR of ice clouds. The vertical thermodynamic profiles from AIRS are interpolated to 109 levels (108 layers) in order to obtain finer vertical resolution. DISORT calculations are carried out for 12 optical thicknesses ranging from 0-10 and 6 effective diameters from 10-60 μm to create a LUT. A granule of MODIS data at 1-km resolution contains nearly 3,000,000 pixels, so creating a new LUT for each MODIS pixel is impractical. The amount of computation time is prohibitive and probably not necessary to obtain sufficient accuracy. Instead, we create a new LUT for each AIRS pixel containing ice clouds and use that LUT to retrieve COT and EPR for any MODIS pixels within the AIRS pixel. This greatly reduces the amount of computation time needed to process one granule of MODIS data.

The LUTs presented in Figure 3 show all the important characteristics that we would expect from the physics of the problem and previous findings. The LUTs show COT sensitivity up to a threshold of about 7. Beyond this limit there is no further sensitivity, because the cloud is essentially opaque to thermal IR radiation. This is also consistent with the findings of Minnis et al. (1995), Inoue (1985), and Wei et al. (2004), who found approximately the same threshold for COT sensitivity. Baum et al. (2000b) observed that $BT_{11} - BT_{12}$ is generally negative for ice clouds with optical thicknesses less than 0.5 and positive for optically thicker clouds. This feature is observed in Figure 3b. Furthermore, small particle sizes are responsible for large BTDs, and this is also

shown in both panels of Figure 3, where the smallest effective radius (5 μm) causes

BTDs as large as 12-13 K. BTDs decrease as the effective radius increases to 30 μm.

There is little sensitivity of BTDs to effective radii larger than 25 μm.

In this section, two IR retrievals will be presented. One retrieval is performed

using the 8.5-μm BT and the (8.5 – 11.0) BTD, referred to as the 8.5/11-μm retrieval.

The other retrieval uses the 11.0-μm BT and the (11.0 – 12.0) BTD and will be referred

to as the 11/12-μm retrieval. Past studies (Baum et al. 2000a, Duda and Spinhirne 1996)

have used these two pairs of channels to derive cloud properties, so we investigate the

use of both pairs in this study.

Figure 12 shows the MODIS cloud phase image for the granule shown in Figure

4. The scene is dominated by water clouds, but a few substantial cirrus clouds are found

in the northern portion of this granule. Some more isolated ice clouds are found in the

southern half of the granule. Figure 13 shows the COT obtained by the IR retrievals and

the MODIS operational retrieval for this granule. In order to be consistent with the

MODIS COT, the IR optical depths are converted to visible optical depth by using the

relation

$$\tau_{vis} = \frac{\beta_{e,vis}}{\beta_{e,IR}} \tau_{IR}, \qquad (22)$$

where τ_{vis} and τ_{IR} are the visible and IR optical depths, respectively, and $\beta_{e,\,vis}$ and $\beta_{e,\,IR}$

are the extinction coefficients for the visible and IR channels, respectively. The IR

retrieval compares reasonably well to MODIS except for the small ice cloud in the
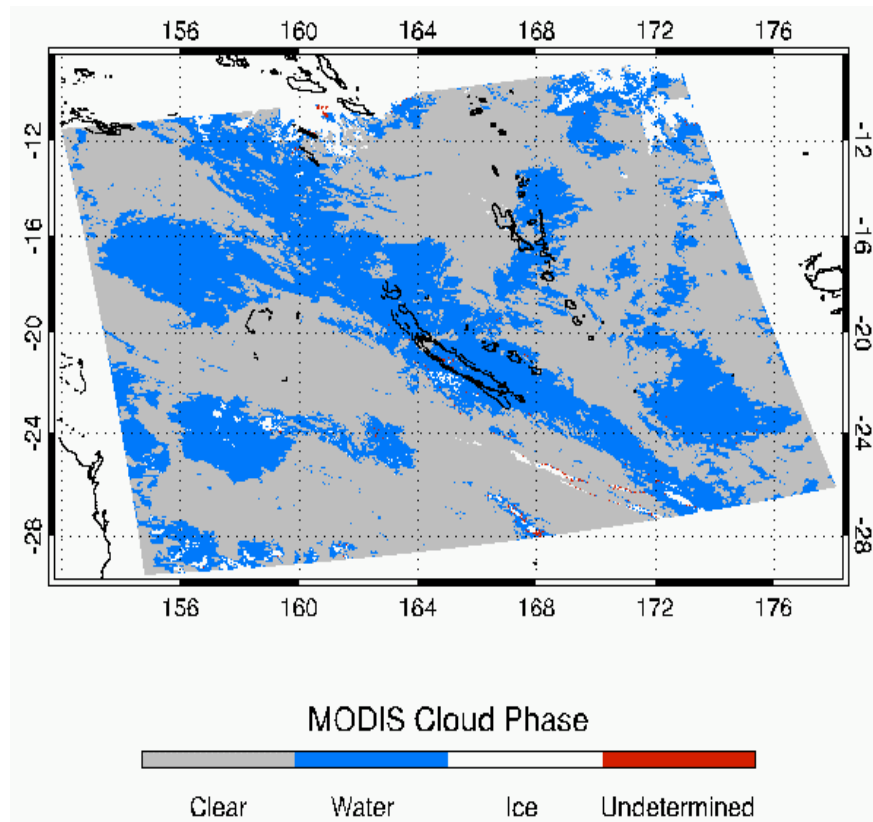
FIG. 12. MODIS cloud phase image for the granule shown in Figure 4.
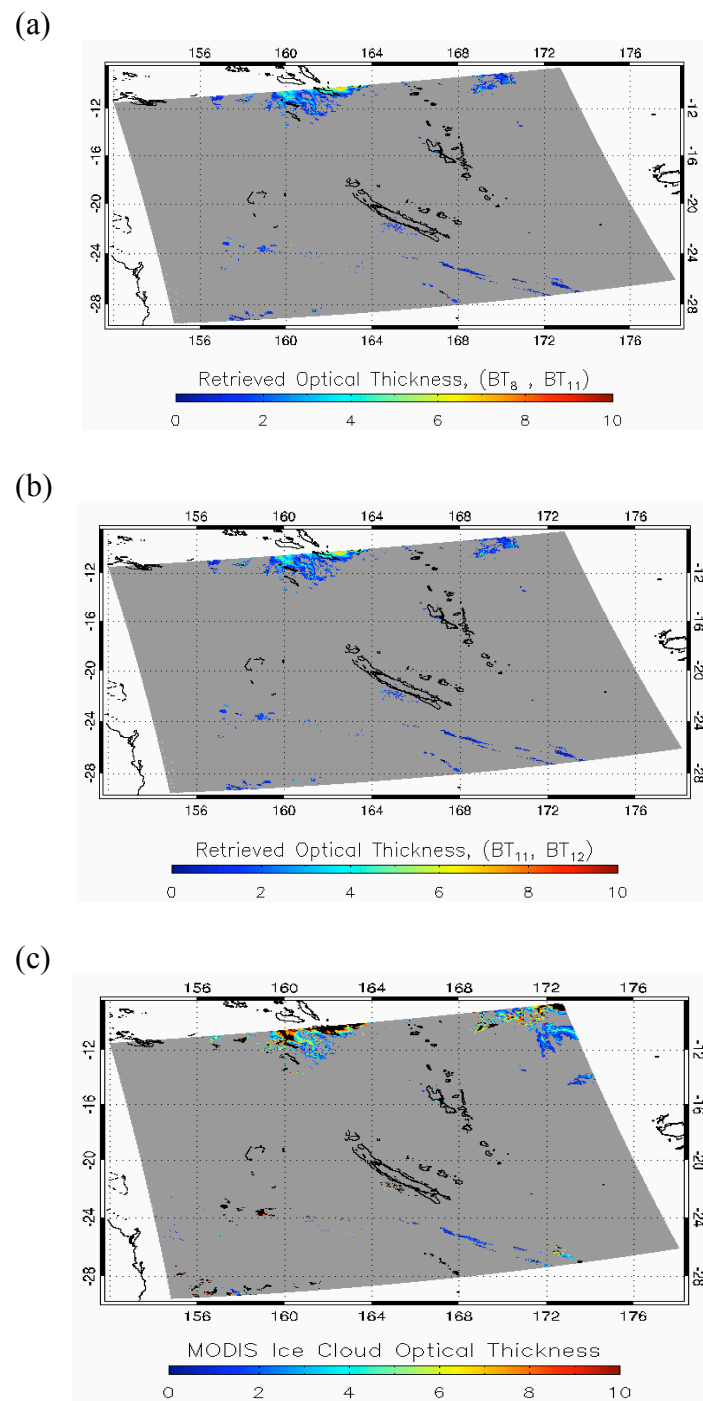
(a)

(b)

(c)

FIG. 13. Ice cloud optical thickness obtained from (a) the 8.5/11.0-μm retrieval, (b) the

11.0/12.0-μm retrieval, and (c) the MODIS operational retrieval for the MODIS granule

shown in Figure 4.

southwest corner of the granule. The IR methods obtain optical thicknesses of

approximately 1, while MODIS obtains values of over 10. Note that the east and west

edges of the granule appear to be truncated in the images of the IR retrieval. This is

merely due to the fact that the AIRS swath width is smaller than the MODIS swath.

Pixels outside the AIRS swath are assigned fill values in our retrieval process.

Scatter plots of the COT from the two IR retrievals reveal that they are consistent

with each other for optical thicknesses less than 10 (Figure 14a). There is considerably

more scatter between the IR and MODIS retrievals (Figure 14b), but the two are fairly

consistent for $\tau < 2$. Once the optical thickness exceeds 2, the two retrievals begin to

diverge. This may be due to saturation of the IR detectors for optically thicker clouds

(Wei et al. 2004).

Figure 15 shows the corresponding images of the effective radius retrievals. In

the model we specified the effective particle size in terms of the effective diameter as

defined in Equation 21. Since the effective radius r_e is defined as

$$r_e = \frac{\int_0^\infty r^3 n(r) dr}{\int_0^\infty r^2 n(r) dr}, \tag{23}$$

where r is the particle radius and $n(r)$ is the particle size distribution, we can easily

convert effective diameter D_e to effective radius by dividing D_e by 2 (King et al. 2004).

The images of the IR effective radius retrievals look quite different when compared to

the MODIS retrieval, but the histograms in Figure 16 better illustrate the differences

between the retrievals. Both IR retrievals found many ice clouds with effective radii

around 20 μm (Fig. 16a and b) while the MODIS effective radius distribution peaks near
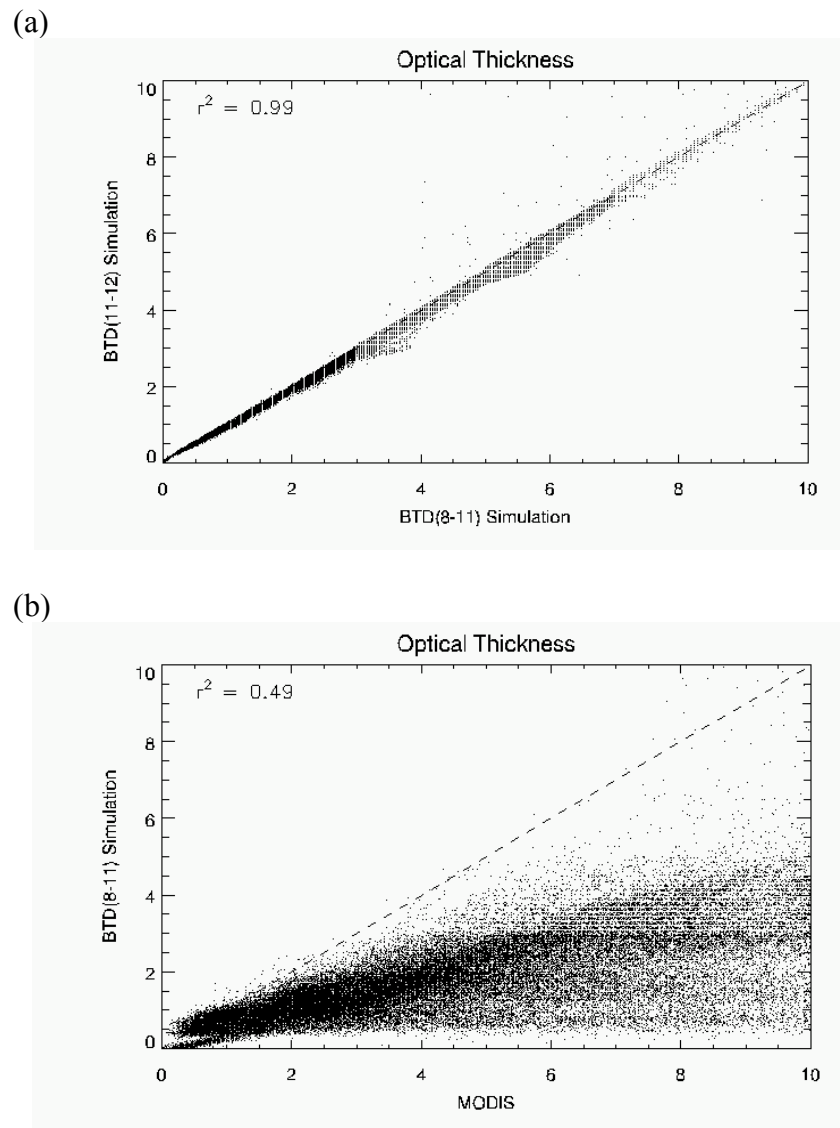
(a)

(b)

FIG. 14. Scatter plots of the ice cloud optical thickness obtained from the (a) 8.5/11- and 11/12-μm retrievals and (b) the 8.5/11-μm and MODIS retrievals for the MODIS granule shown in Figure 4.

(a)

Retrieved Effective Particle Radius (microns), (BT_8, BT_{11})

(b)

Retrieved Effective Particle Radius (microns), (BT_{11}, BT_{12})

(c)

MODIS Effective Ice Particle Radius (microns)

FIG. 15. Ice cloud effective radii obtained from (a) the 8.5/11.0-μm retrieval, (b) the 11.0/12.0-μm retrieval, and (c) the MODIS operational retrieval for the MODIS granule shown in Figure 4.

(a)

(b)

(c)
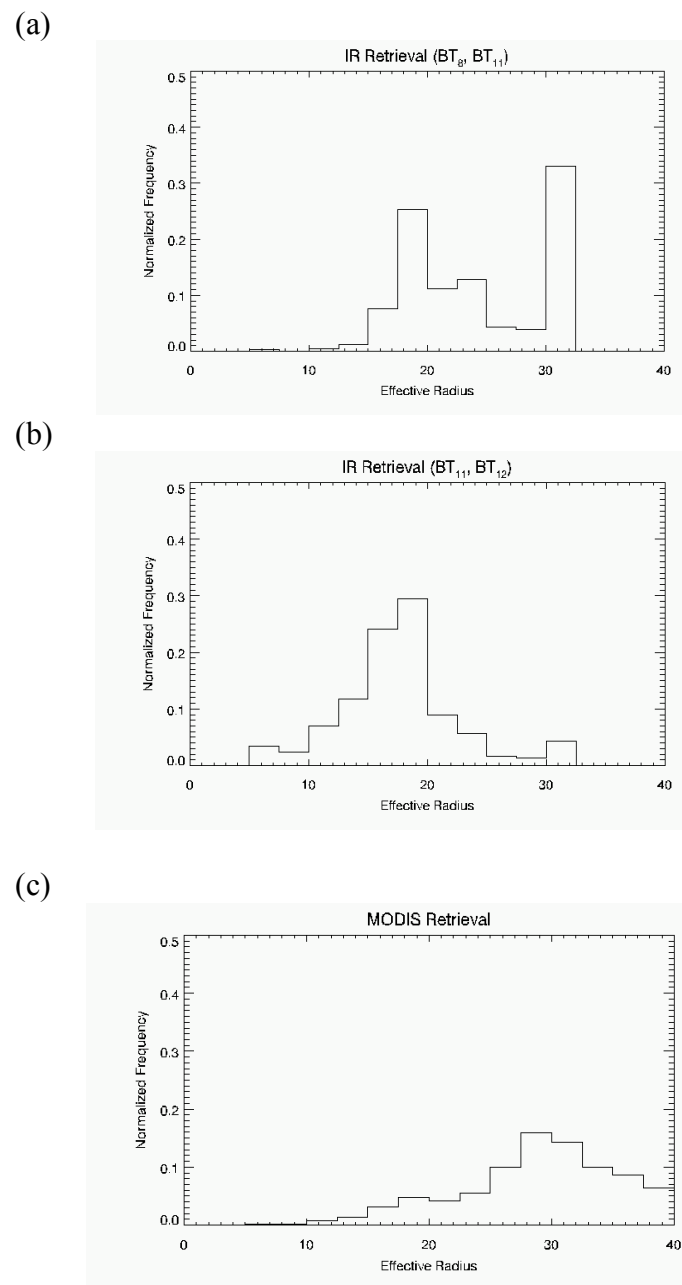
FIG. 16. Histograms of the ice cloud effective particle radii obtained from (a) the 8.5/11-μm retrieval, (b) the 11/12-μm retrieval, and (c) the MODIS operational retrieval for the MODIS granule shown in Figure 4.

30 μm (Fig. 16c). The MODIS peak is much less pronounced and the distribution is

smoother than that of the IR retrievals. The 11/12-μm retrieval found slightly more

clouds with effective radii smaller than 15 μm than either of the other two retrievals.

For the 8.5/11-μm retrieval, a large peak is seen near 30 μm where many observations

fell outside the valid range of the LUT (Fig. 16a), but this could be expected because the

MODIS retrieval finds a significant number of clouds with effective radii larger than 30

μm. The maximum retrievable effective radius in this study is 30 μm, and any radii

larger than this limit are retrieved as 30 μm. This shows up in the histogram as the large

peak at 30 μm, but the peak is much less pronounced for the 11/12-μm retrieval. In this
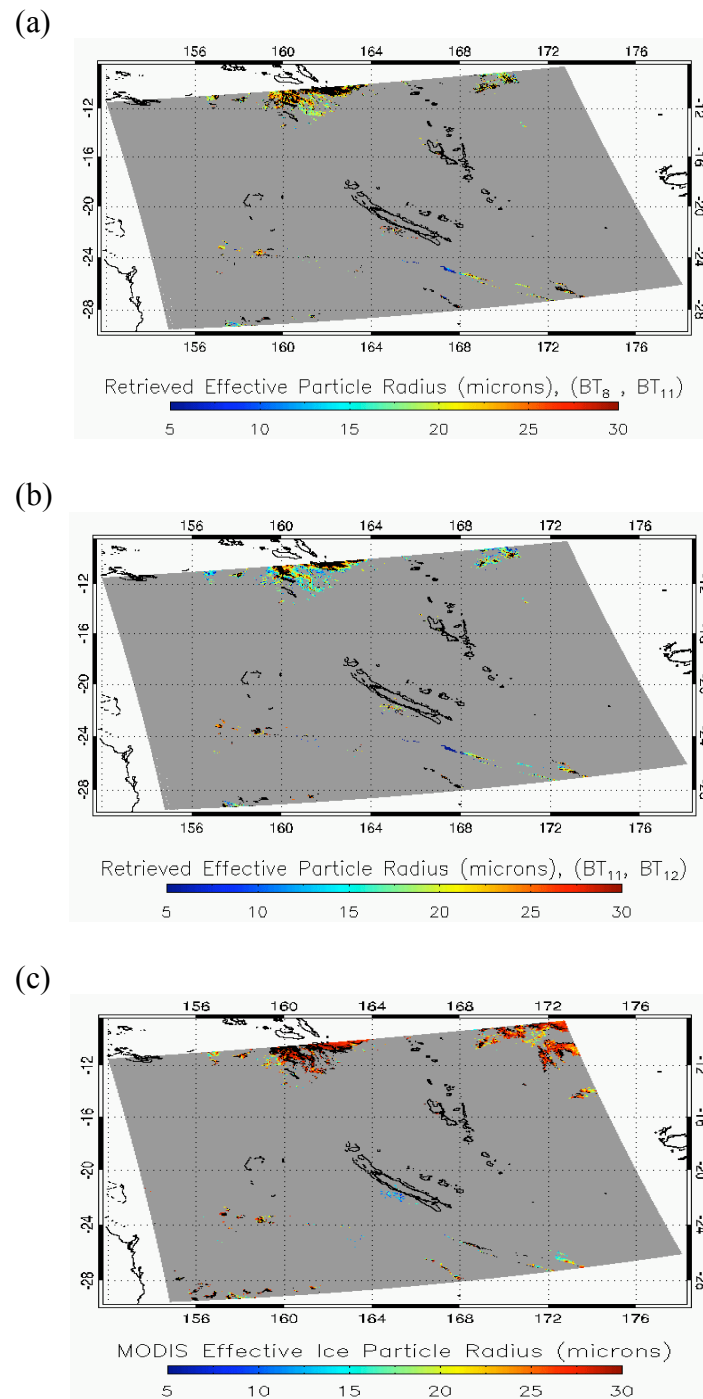
case, it seems that the 8.5/11-μm retrieval better matches the MODIS retrieval than the

11/12-μm retrieval.

The IR retrieval was performed on another MODIS granule that was obtained on

26 July, 2006, over the tropical Pacific Ocean just to the west of the South American

coast. A false-color composite image of the granule is shown in Figure 17a, and the

MODIS cloud phase image is shown in Figure 17b. The blue colors in Figure 17a

correspond very well to the pixels flagged as ice cloud in the MODIS cloud phase

image. The ice clouds in this granule are more widespread, stretching from the

northwest to the southeast corners of the granule. There appears to be a large amount of

cloud layer overlap, with high altitude cirrus clouds (blue) overlaying low level water

clouds (green).

Figure 18 shows the retrieved COT for this granule. The two IR retrievals (Fig.

18a and b) appear to match very well with each other, and compare reasonably well to

(a)

MYD021KM.A2006207.2025.005.2006209042912.hdf
July 26, 2006

(b)

MODIS Cloud Phase

Clear   Water   Ice   Undetermined

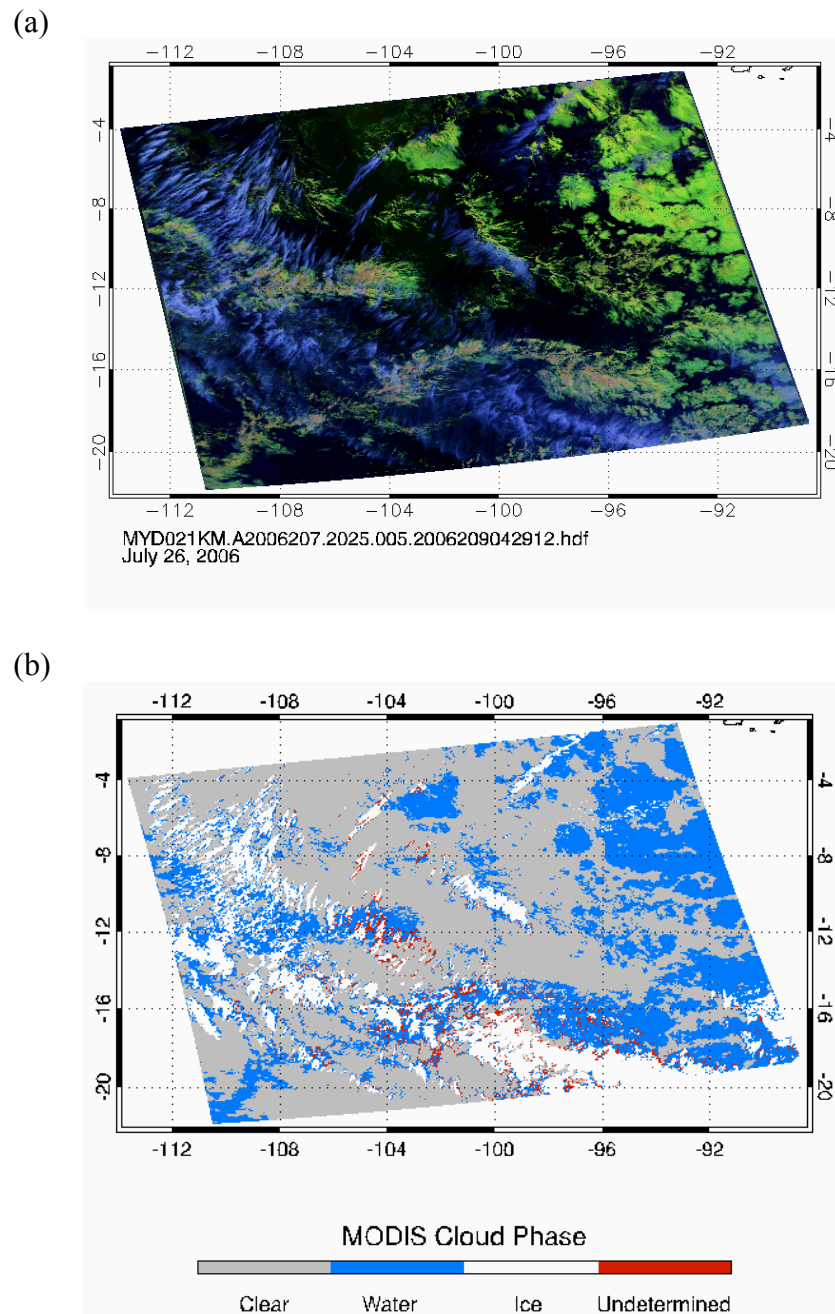FIG. 17. Images of (a) a 0.65- (red), 2.13- (green) and 11.0-μm (blue) false-color composite and (b) the MODIS cloud mask for a MODIS granule obtained on 26 July, 2006, over the tropical Pacific Ocean.
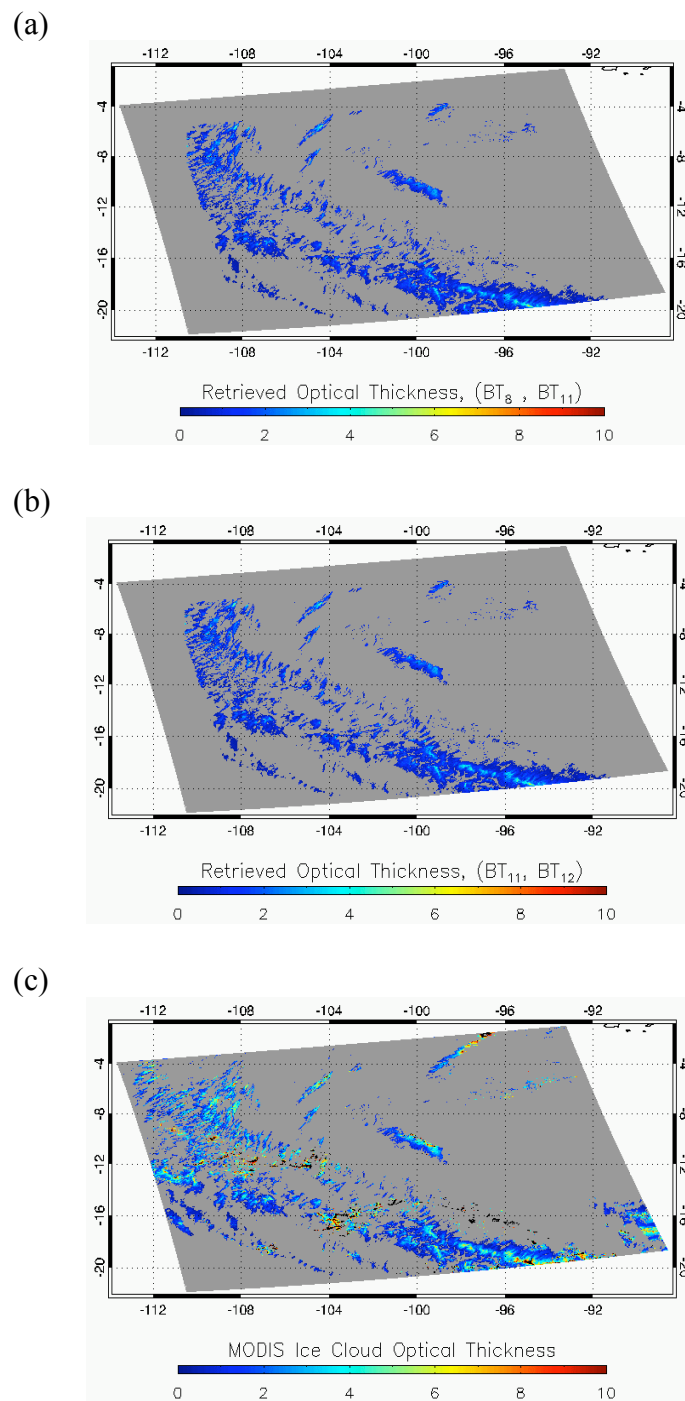
(a)

(b)

(c)

FIG. 18. Ice cloud optical thickness obtained from (a) the 8.5/11.0-μm retrieval, (b) the

11.0/12.0-μm retrieval, and (c) the MODIS operational retrieval for the MODIS granule

shown in Figure 15.

the MODIS image (Fig. 18c). Inspection of these images reveals that the MODIS

retrieval obtains slightly higher values for the COT, with some values greater than 10.

The scatter plots in Figure 19 again show that the two IR retrievals are consistent with

each other. MODIS does indeed find higher COT values (Fig. 19b) and we find the

same pattern here as in Figure 14. While there is a considerable amount of scatter in

Figure 19b, there are many points that fall on or near the one-to-one ratio line up to

optical thicknesses around 2. After this threshold, the IR and MODIS COT retrievals

diverge.

The EPR retrievals for the same granule are shown in Figure 20. The two IR

retrievals look pretty similar, although it appears that the 8.5/11-μm retrieval finds more

large ice particles. This is confirmed in Figure 21a and b, as the histograms show a

larger peak at 30 μm for the 8.5/11-μm retrieval than the 11/12-μm retrieval. The EPR

distributions for the two IR retrievals look similar, but the 11/12-μm retrieval again has a

slightly larger peak at 20 μm and a smaller peak for particles over 30 μm than the

8.5/11-μm retrieval. Again, compared to MODIS, the histograms reveal that the IR

retrieval tends to find smaller ice particles. The MODIS distribution tends to be

smoother and peaks between 25 and 30 μm while the IR EPR retrievals peak sharply

around 15-20 μm.

b. Discussion

In Section 3, we investigated the errors associated with biases in the

thermodynamic profiles and the surface temperature. For cloudy BT simulations, cloud

(a)

(b)
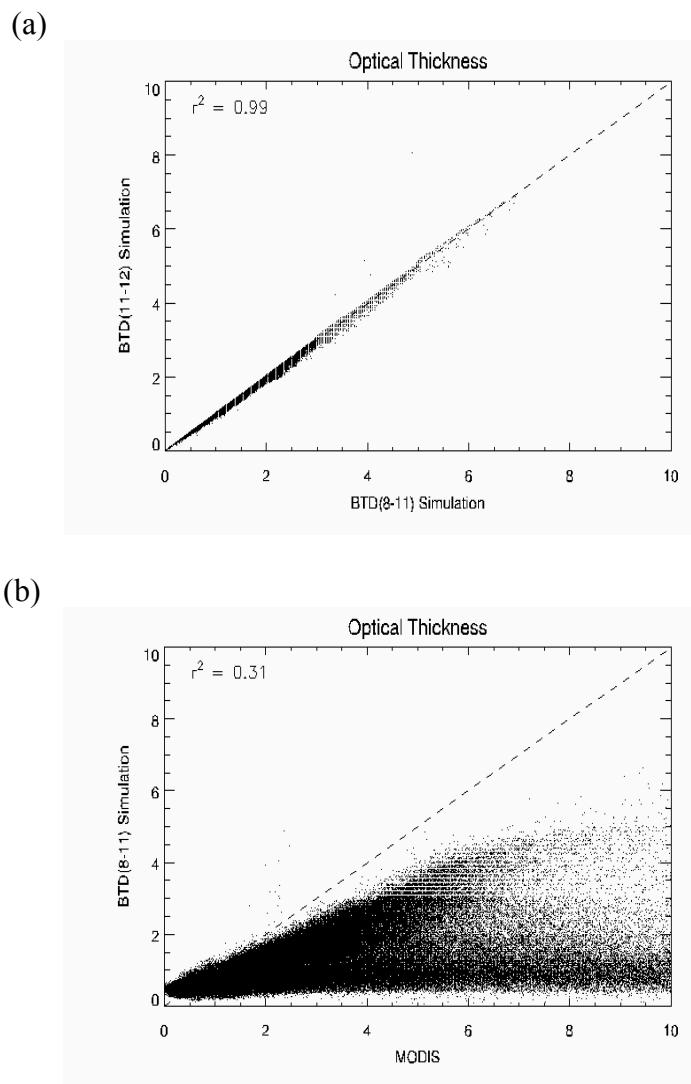
FIG. 19. Scatter plots of the ice cloud optical thickness obtained from the (a) 8.5/11- and

11/12-μm retrievals and (b) the 8.5/11-μm and MODIS retrievals for the MODIS

granule shown in Figure 15.

(a)

(b)

(c)

FIG. 20. Ice cloud effective radii obtained from (a) the 8.5/11.0-μm retrieval, (b) the

11.0/12.0-μm retrieval, and (c) the MODIS operational retrieval for the MODIS granule

shown in Figure 15.

(a)

IR Retrieval (BT$_8$, BT$_{11}$)

(b)

IR Retrieval (BT$_{11}$, BT$_{12}$)

(c)
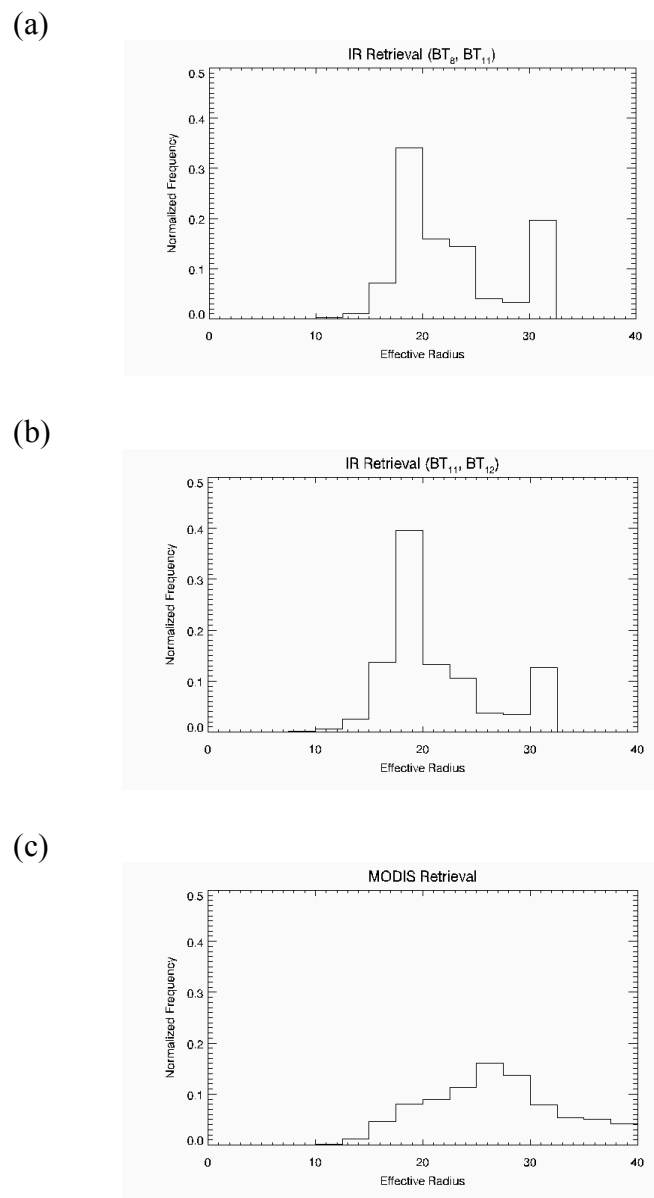
MODIS Retrieval

FIG. 21. Histograms of the ice cloud effective particle radii obtained from (a) the 8.5/11-μm retrieval, (b) the 11/12-μm retrieval, and (c) the MODIS operational retrieval for the MODIS granule shown in Figure 4.

top temperature (CTT) is another possible source of error. For cloudy BT simulations,

we interpolate the vertical profiles to 109 levels (108 layers) in order to get better

vertical resolution. A cloud is then inserted into one of the model layers. The cloud

temperature is assumed to equal the average temperature of the layer in which it is

located. The AIRS CTP product is used to determine this layer instead of the CTT

product simply because pressure decreases monotonically with height while temperature

does not necessarily have this convenient characteristic. It is possible to get a unique

cloud layer using the cloud top pressure, while using CTT may produce multiple

solutions if there is a temperature inversion in the troposphere. Therefore we next

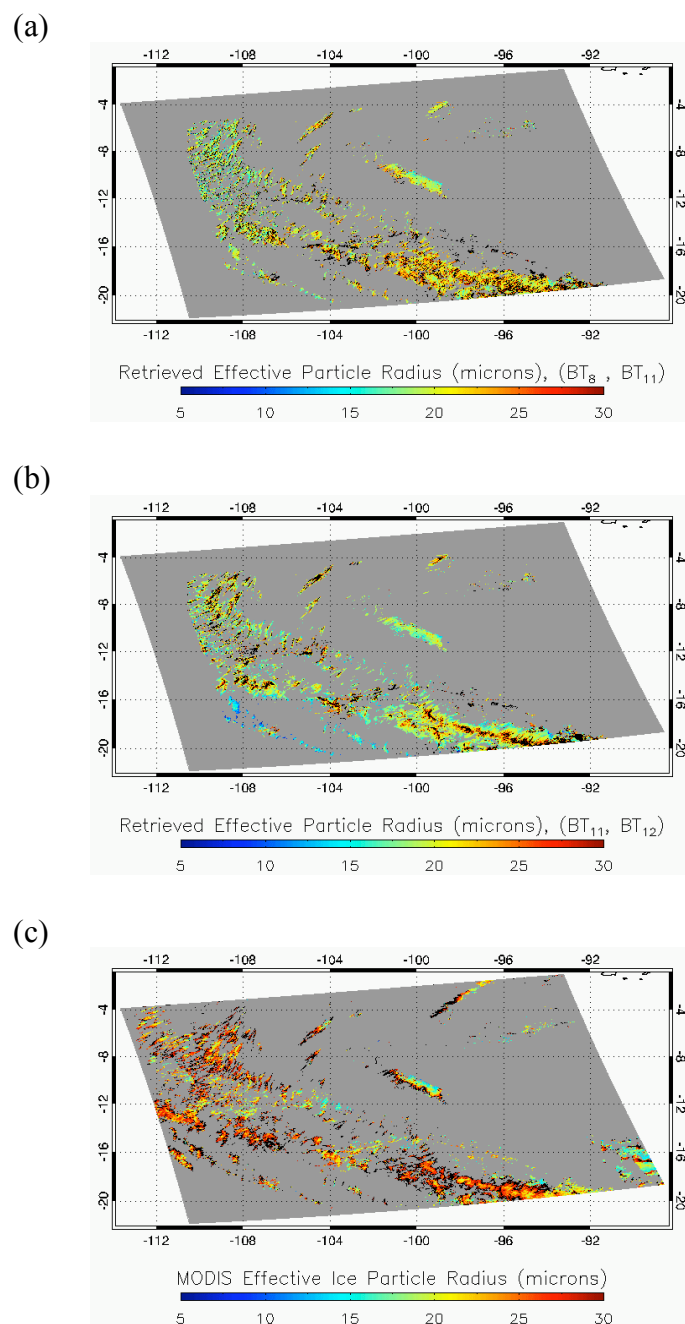investigate the effects of variations in both the CTT and CTP on the cloud property

retrieval.

Figures 22 and 23 show sample LUTs for the 8.5/11-μm and 11/12-μm

retrievals, respectively. These tables were created for one pixel of the AIRS granule

shown in Figure 8, and the MODIS-observed BTs and BTDs within the AIRS pixel are

plotted on top of the LUTs. These figures illustrate how errors in the CTP will affect the

IR retrievals. In the model, CTP is used indirectly to get CTT, and both values are

displayed in each panel of Figures 22 and 23. Notice how the shape of the LUT changes

with changes in the CTP (and therefore the CTT also). In this case, a 50 mb difference

in CTP translates into a 10 K difference in cloud temperature. It is evident from Figures

22 and 23 that an inaccurate cloud temperature will cause errors in the inferred cloud

properties, and some observations may not fall within the valid range of the LUT.

Although not explicitly considered in this study, the geometrical thickness of a

(a)

(b)

(c)

FIG. 22. Lookup tables for the 8.5/11-μm retrieval where the average cloud temperature is approximately (a) 232 K, (b) 221 K, and (c) 212 K. MODIS observations are plotted over the lookup tables.
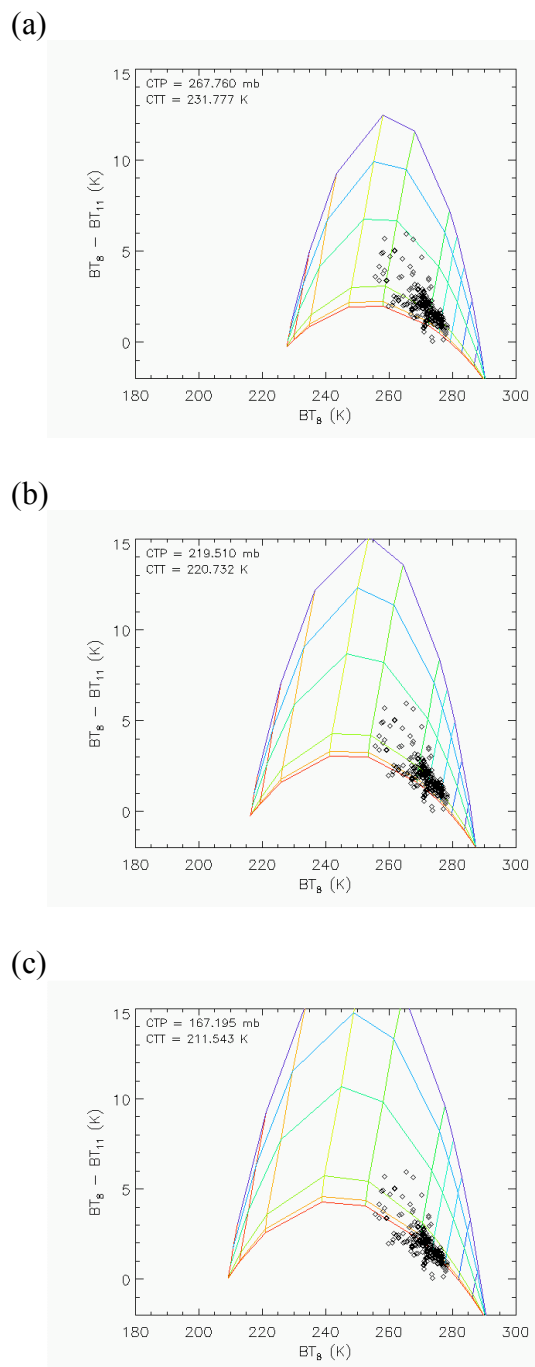
(a)

(b)

(c)

FIG. 23. Lookup tables for the 11/12-μm retrieval where the average cloud temperature is approximately (a) 232 K, (b) 221 K, and (c) 212 K. MODIS observations are plotted over the lookup tables.
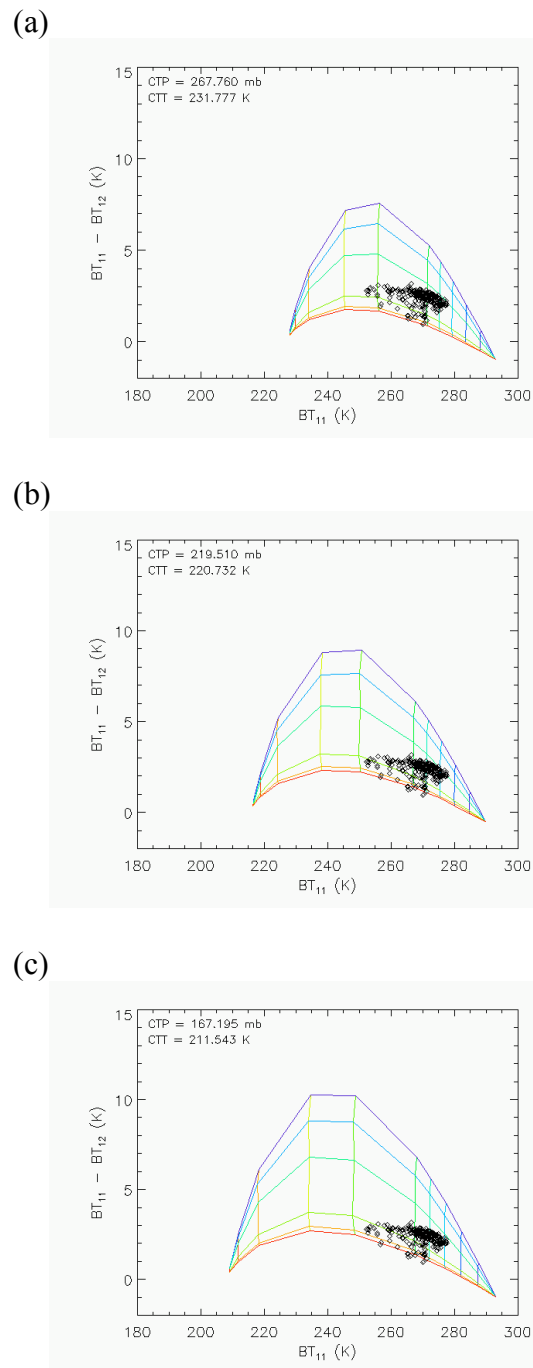
cloud layer can potentially have a significant impact. In our model we chose to interpolate the vertical thermodynamic profiles to obtain relatively high vertical resolution in order to accurately approximate the CTT. Creating geometrically thin layers is a side effect of increasing the vertical resolution. In our model, the geometrical thickness of the layers varies but is generally less than 1 km. Therefore we have implicitly assumed that clouds in the model extend no more than about 1 km in the vertical direction. This can potentially cause problems for clouds that are both optically thin and geometrically thick. Since we determine the appropriate cloud layer by matching the CTP, as opposed to the cloud base pressure, to the vertical pressure profile, the simulated BT will be underestimated for a cloud with a geometrical thickness greater than 1 km. The emission due to cloud particles in warmer layers closer to the surface is not considered. It is emphasized that only cloud emission may suffer from this effect, but the molecular absorption and emission are still adequately simulated. Additional work needs to be performed in order to determine the importance of cloud geometrical thickness in RT calculations, but Hong et al. (2006) provide some insight into this problem. Their study found that variations in cloud geometrical thickness may cause 11.0-μm BT variations as large as 8 K for ice clouds with optical thicknesses of about 5 and altitudes of 12 km. The results for the 8.5- and 12.0-μm bands were similar, with optically thin clouds generally being affected the most. Since the IR retrieval used in this study is applicable to optically thin ice clouds, the effects of cloud geometrical thickness clearly deserve more attention.

Partial cloudiness and multilayer clouds are common problems in cloud property retrievals. In this study we assumed the AIRS and MODIS FOVs were completely filled with a one-layer homogeneous ice cloud. Because of this assumption, any partially cloudy MODIS pixels will likely have higher BTs than completely cloudy pixels, resulting in underestimation of COT. The amount of scatter in Figures 14 and 19 could be reduced by limiting the IR retrieval to cases where the cloud amount is at least 90%. Mixed phase clouds will cause problems because the radiative transfer calculations are performed assuming ice is the only cloud constituent. Multilayer cloud scenes are also troublesome, especially when a warm water cloud lies below an optically thin cirrus cloud. This problem could be mitigated somewhat by using the new MODIS multilayer cloud detection algorithm to flag pixels containing multiple cloud layers. Limiting the IR retrieval to single-layer ice clouds is essential, because the model was not constructed to handle multiple cloud layers.

In this study, the IR retrieval was limited to FOVs over an ocean surface, because the spectral emissivity of the ocean is fairly constant in space and time over the thermal IR spectral region. IR retrievals over land are possible but are hindered by the fact that land surfaces are not as uniform as an ocean surface. Dry soil, moist soil, snow, sand, and vegetation all have different spectral emissivities, and this must be accounted for when attempting retrievals over land.

Although many steps were taken to reduce the amount of time needed to perform the cloud property retrieval for one MODIS granule, the amount of time needed to process one granule is still much more than the requirement for real-time processing.

Depending on the amount ice cloud coverage, one granule may take several hours or even days to process. Most of the processing time is spent performing RT calculations. A two-stream RT code could be used in place of DISORT to decrease execution time, but the accuracy of the model with the two-stream code would first need to be assessed.

5. DISCUSSION AND CONCLUSIONS

The IR atmospheric window between 8-12 μm is important for weather and climate change studies, because longwave emission peaks within this spectral region and is therefore a major cooling mechanism for our planet. Ice clouds strongly absorb this radiation and emit it back to the surface, thus trapping some of the energy that would otherwise escape to space. This effect makes ice clouds important for weather and climate change studies as well, and much effort has been placed on understanding the optical and microphysical properties of ice clouds, which will help the scientific community determine their radiative forcing.

In this study we further explored the use of thermal IR channels in the atmospheric window to retrieve the COT and EPR of ice clouds. These two quantities, along with IWP and cloud fraction, are widely used to determine cloud radiative forcing. The advantage of using channels in the IR spectral region is that retrievals involving them are not limited to daytime use only and thus can potentially complement daytime methods to provide a more complete dataset of cloud properties. MODIS provides three bands in the 8-12-μm spectral region at relatively high spatial resolution, making it an excellent instrument for IR cloud property retrieval research.

The sensitivity study described in Section 3 examined the effects of small variations in the temperature profile, moisture profile, and surface temperature. In general, reasonable biases affected the clear-sky TOA BTs by less than about 3 K. This suggests that small variations in these three input parameters over an AIRS or MODIS pixel will not strongly affect the simulated BTs. It is more difficult to determine exactly

how these variations affect the retrieval of COT and EPR, because the impact depends on the COT itself. For example, an error in the surface temperature will impact the retrieval of an optically thin cloud more than an optically thicker cloud, because an optically thicker cloud is more opaque to surface emission.

While the IR retrieval in this study suffers from the familiar problems of partial cloudiness, cloud overlap, and vertically inhomogeneous clouds, the results presented here look promising. The IR COT retrieval compares fairly well to MODIS, although the results begin to diverge for optical thicknesses greater than about 2. The IR retrieval also tends to find more ice particles with effective radii near 20 μm while MODIS effective radii retrievals peak less sharply around 25-30 μm. The IR retrieval method in this study is applicable to ice clouds with optical thicknesses less than about 7 and effective radii less than about 25 μm. Beyond these limits there is no further sensitivity of this method to COT and EPR.

More work needs to be done to characterize the effects of multiple cloud layers, partially cloudy pixels, and vertically inhomogeneous clouds on this retrieval. It is likely that these situations are responsible for some of the discrepancy between the IR and MODIS retrievals, since these cases were not filtered out before performing the IR retrieval. Furthermore, the model requires fairly accurate surface skin temperatures and cloud top pressures as input, and the calculation of these parameters is suspect for less than ideal conditions, such as in the presence of precipitating clouds. Although the IR retrieval explored in this study is limited to a subset of clouds, it can provide valuable nighttime cloud properties. This will ultimately help provide a more complete climate

record with which to study cloud radiative forcing and the role of clouds in climate

change.

REFERENCES

Ackerman, S. A., K. I. Strabala, W. P. Menzel, R. A. Frey, C. C. Moeller, and L. E. Gumley, 1998: Discriminating clear sky from clouds with MODIS. *J. Geophys. Res.*, **103**, 32414-32157.

——, W. L. Smith, J. D. Spinhirne, and H. E. Revercomb, 1990: The 27-28 October 1986 FIRE IFO cirrus case study: Spectral properties of cirrus clouds in the 8-12 μm window. *Mon. Wea. Rev.*, **118**, 2377-2388.

Aumann, H. H., M. T. Chahine, C. Gautier, M. D. Goldberg, E. Kalnay, L. M. McMillin, H. Revercomb, P. W. Rosenkranz, W. L. Smith, D. H. Staelin, L. L. Strow, and J. Susskind, 2003: AIRS/AMSU/HSB on the Aqua mission: Design, science objectives, data products, and processing systems. *IEEE Trans. Geosci. Remote Sens.*, **41**, 253-264.

Baum, B. A., P. Yang, A. J. Heymsfield, S. Platnick, M. D. King, Y.-X. Hu, and S. T. Bedka, 2005: Bulk scattering properties for the remote sensing of ice clouds. Part II: Narrowband models. *J. Appl. Meteor.*, **44**, 1896-1911.

——, D. P. Kratz, P. Yang, S. C. Ou, Y.-X. Hu, P. F. Soulen, and S.-C. Tsay, 2000a: Remote sensing of cloud properties using MODIS airborne simulator imagery during SUCCESS 1. Data and models. *J. Geophys. Res.*, **105**, 11767-11780.

——, P. F. Soulen, K. I. Strabala, M. D. King, S. A. Ackerman, W. P. Menzel, and P. Yang, 2000b: Remote sensing of cloud properties using MODIS airborne simulator imagery during SUCCESS 2. Cloud thermodynamic phase. *J. Geophys. Res.*, **105**, 11781-11792.

Chahine, M. T., H. Aumann, M. Goldberg, L. McMillin, P. Rosenkranz, D. Staelin, L. Strow, and J. Susskind, 2001: AIRS-team retrieval for core products and geophyisical parameters. *AIRS Level 2 Algorithm Theoretical Basis Document Version 2.2*, 190 pp.

Chandresekhar, S., 1960: *Radiative Transfer*. New York, Dover, 393 pp.

Duda, D. P., and J. D. Spinhirne, 1996: Split-window retrieval of particle size and optical depth in contrails located above horizontally inhomogeneous ice clouds. *Geophys. Res. Lett.*, **23**, 3711-3714.

Foot, J. S., 1988: Some observations of the optical properties of clouds: II Cirrus. *Quart. J. Roy. Meteor Soc.*, **114**, 145-164.

Francis, P. N., A. Jones, R. W. Saunders, K. P. Shine, A. Slingo, and Z. Sun, 1994: An observational and theoretical study of the radiative properties of cirrus: Some results from ICE'89. *Quart. J. Roy. Meteor. Soc.*, **120**, 809-848.

Fu, Q., and K. N. Liou, 1992: On the correlated *k*-distribution method for radiative transfer in nonhomogeneous atmospheres. *J. Atmos. Sci.*, **49**, 2139-2156.

Hong, G., P. Yang, H.-L. Huang, B. A. Baum, Y. X. Hu, and S. Platnick, 2006: The sensitivity of ice cloud optical and microphysical passive satellite retrievals to cloud geometrical thickness. *IEEE Trans. Geosci. Remote Sens.*, submitted.

Hu, Y.-X., B. Wielicki, B. Lin, G. Gibson, S.-C. Tsay, K. Stamnes, and T. Wong, 2000: δ-fit: A fast and accurate treatment of particle scattering phase functions with weighted singular-value decomposition least-squares fitting. *J. Quant. Spectrosc. Radiat. Transfer*, **65**, 681-690.

Huang, H.-L., P. Yang, H. Wei, B. A. Baum, Y. Hu, P. Antonelli, and S. A. Ackerman, 2004: Inference of ice cloud properties from high spectral resolution infrared observations. *IEEE Trans. Geosci. Remote Sens.*, **42**, 842-853.

Inoue, T., 1985: On the temperature and effective emissivity determination of semi-transparent cirrus clouds by bi-spectral measurements in the 10 μm window region. *J. Meteor. Soc. Japan.*, **63**, 88-98.

Kidder, S. Q., and T. H. Vonder Haar, 1995: *Satellite Meteorology: An Introduction*. San Diego, Academic Press, 466 pp.

King, M. D., S. Platnick, P. Yang, G. T. Arnold, M. A. Gray, J. C. Riedi, S. A. Ackerman, and K.-N. Liou, 2004: Remote sensing of liquid water and ice cloud optical thickness and effective radius in the Arctic: Application of airborne multispectral MAS data. *J. Atmos. Oceanic Technol.*, **21**, 857-875.

———, W. P. Menzel, Y. J. Kaufman, D. Tanre, B.-C. Gao, S. Platnick, S. A. Ackerman, L. A. Remer, R. Pincus, and P. A. Hubanks, 2003: Cloud and aerosol properties, precipitable water, and profiles of temperature and water vapor from MODIS. *IEEE Trans. Geosci. Remote Sens.*, **41**, 442-458.

———, S.-C. Tsay, S. Platnick, M. Wang, and K. N. Liou, 1997: Cloud retrieval algorithms for MODIS: Optical thickness, effective particle radius, and thermodynamic phase. *MODIS Algorithm Theoretical Basis Document No. ATBD-MOD-05*, 79 pp.

———, D. D. Herring, and D. J. Diner, 1995: The Earth Observing System: A space-based program for assessing mankind's impact on the global environment. *Optics and Photonics News*, **6**, 34-39.

Kratz, D. P., 1995: The correlated *k*-distribution technique as applied to the AVHRR channels. *J. Quant. Spectrosc. Radiat. Transfer*, **53**, 501-517.

Liou, K. N., 2002: *An Introduction to Atmospheric Radiation: Second Edition*, Amsterdam, Academic Press, 583 pp.

———, 1974: On the radiative properties of cirrus in the window region and their influence on remote sensing of the atmosphere. *J. Atmos. Sci.*, **31**, 522-532.

McFarquhar, G. M., A. J. Heymsfield, J. Spinhirne, and B. Hart, 2000: Thin and subvisual tropopause tropical cirrus: Observations and radiative impacts. *J. Atmos. Sci.*, **57**, 1841-1853.

Menzel, W. P., B. A. Baum, K. I. Strabala, and R. A. Frey, 2002: Cloud top properties and cloud phase algorithm theoretical basis document. *MODIS Algorithm Theoretical Basis Document No. ATBD-MOD-04.*, 61 pp.

Meyer, K., P. Yang, and B.-C. Guo, 2004: Optical thickness of tropical cirrus clouds derived from the MODIS 0.66- and 1.375-μm channels. *IEEE Trans. Geosci. Remote Sens.*, **42**, 833-841.

Minnis, P., D. A. Kratz, J. A. Coakley, M. D. King, D. Garber, P. Heck, S. Mayor, W. L. Smith, D. F. Young, and R. Arduini, 1995: Cloud optical property retrieval. *Clouds and the Earth's Radiant Energy System (CERES) Algorithm Theoretical Basis Document. Volume III: Cloud Analyses and Determination of Improved Top of Atmosphere Fluxes (Subsystem 4)*, edited by CERES Science Team, 42 pp.

Nakajima, T. and M. D. King, 1990: Determination of the optical thickness and effective particle radius of clouds from reflected solar radiation measurements. Part I: theory. *J. Atmos. Sci.*, **47**, 1878-1893.

Nasiri, S., B. A. Baum, A. J. Heymsfield, P. Yang, M. R. Poellot, D. P. Kratz, and Y.-X. Hu, 2002: The development of midlatitude cirrus models for MODIS using FIRE-I, FIRE-II, and ARM in situ data. *J. Appl. Meteor.*, **41**, 197-217.

Platnick, S., M. D. King, S. A. Ackerman, W. P. Menzel, B. A. Baum, J. C. Riedi, and R. A. Frey, 2003: The MODIS cloud products: Algorithms and examples from Terra. *IEEE Trans. Geosci. Remote Sens.*, **41**, 459-472.

Potter, J. F., 1970: The delta function approximation in radiative transfer theory. *J. Atmos. Sci.*, **27**, 943-949.

Ramanathan, V., R. D. Cess, E. F. Harrison, P. Minnis, B. R. Barkstrom, E. Ahmad, and D. Hartmann, 1989: Cloud-radiative forcing and climate: Results from the Earth Radiation Budget Experiment. *Science*, **243**, 57-63.

Stamnes, K., S.-C. Tsay, W. Wiscombe, and K. Jayaweera, 1988: Numerically stable algorithm for discrete-ordinate-method radiative transfer in multiple scattering and emitting layered media. *Appl. Opt.*, **27**, 2502-2509.

Strabala, K. I., S. A. Ackerman, and W. P. Menzel, 1994: Cloud properties inferred from 8-12-μm data. *J. Appl. Meteor.*, **33**, 212-229.

Susskind, J., C. D. Barnet, and J. M. Blaisdell, 2003: Retrieval of atmospheric and surface parameters from AIRS/AMSU/HSB data in the presence of clouds. *IEEE Trans. Geosci. Remote Sens.*, **41**, 390-409.

Takano, Y. and K.-N. Liou, 1989: Solar radiative transfer in cirrus clouds. Part I: Single-scattering and optical properties of hexagonal ice crystals. *J. Atmos. Sci.*, **46**, 3-19.

Wei, H., P. Yang, J. Li, B. A. Baum, H.-L. Huang, S. Platnick, Y. Hu, and L. Strow, 2004: Retrieval of semitransparent ice cloud optical thickness from Atmospheric Infrared Sounder (AIRS) measurements. *IEEE Trans. Geosci. Remote Sens.*, **42**, 2254-2267.

Wielicki, B. A., R. D. Cess, M. D. King, D. A. Randall, and E. F. Harrison, 1995: Mission to planet Earth: Role of clouds and radiation in climate. *Bull. Am. Meteorol. Soc.*, **76**, 2125-2153.

Wiscombe, W. J., 1977: The delta-M method: Rapid yet accurate radiative flux calculations for strongly asymmetric phase functions. *J. Atmos. Sci.*, **34**, 1408-1422.

Wyser, K. and P. Yang, 1998: Average ice crystal size and bulk short-wave single-scattering properties of cirrus clouds. *Atmos. Res.*, **49**, 315-335.

Yang, P., H. Wei, H.-L. Huang, B. A. Baum, Y. X. Hu, G. W. Kattawar, M. I. Mishchenko, and Q. Fu, 2005: Scattering and absorption property database for nonsperical ice particles in the near- through far-infrared spectral region. *Appl. Opt.*, **44**, 5512-5523.

———, B. A. Baum, A. J. Heymsfield, Y. X. Hu, H.-L. Huang, S.-C. Tsay, and S. Ackerman, 2003: Single-scattering properties of droxtals. *J. Quant. Spectrosc. Radiat. Transfer*, **79-80**, 1159-1169.

———, K. N. Liou, and W. P. Arnott, 1997: Extinction efficiency and single-scattering albedo for laboratory and natural cirrus clouds. *J. Geophys. Res.*, **102**, 21825-21835.

VITA

Biography

Christopher Rogers Yost was born in San Antonio, TX, and has been a proud Texan for over 20 years. He graduated from Douglas MacArthur High School in 2000 and enrolled in Texas A&M University in the fall of the same year. In June 2006, he moved to Hampton, VA, where his permanent address is 1006 Cameo Dr., Hampton, VA 23666.

Educational Background

B.S., Meteorology, Texas A&M University, December 2004.

M.S., Atmospheric Sciences, Texas A&M University, December 2006.